The Ambiguity Costs of Climate Change

Frances C. Moore,[1*] Matias Solorza[2] and Benjamin Collier,[3]

[1]Department of Environmental Science and Policy, University of California Davis
[2] Department of Economics, University of California Davis
[3] Department of Risk and Insurance, University of Wisconsin-Madison

*To whom correspondence should be addressed; e-mail: fmoore@ucdavis.edu.

Abstract

Weather risks are fundamentally more difficult to manage under climate change because past experience of weather is potentially unrepresentative of current exposure. The possibility of climate change acts as a global information shock, degrading utility of the historic weather record with implications for actors across the economy making weather-contingent decisions. Here we quantify these ambiguity-related costs for a major climate risk, namely urban flood damages in the United States. Using daily rainfall for 151 US cities from 1970 to 2024, we contrast the 2024 extreme rainfall distribution under a Bayesian model that assumes the rainfall distribution is stationary with one that allows for time-evolving GEV parameters, consistent with the possibility of a changing climate. Estimated tail risks increase notably when allowing the climate to evolve: the 99th percentile rainfall event is larger in 89% of the cities in our sample. Economic costs of these tail risks are amplified by convex damage functions, which we estimate at the city level using flood insurance policy and claim data. Modeling aggregate losses for portfolios at the city, state, regional, and national level, we find geographic diversification only modestly abates these tail risks: the 99th percentile loss event is 4-5 times larger when accounting for evolving climate risk at all levels of aggregation. In a private insurance market these much larger tail risks would substantially increase required capital holdings and the cost of supplying insurance. Our analysis highlights the substantial economic costs of climate change-driven ambiguity in weather extremes and sheds light on recent volatility in US insurance markets.

1 Introduction

The costs of anthropogenic climate change are now well established. Altered weather patterns are already affecting important social and economic outcomes around the world, with impacts likely to grow over time as global warming intensifies. Outcomes as diverse as mortality, learning, labor productivity, crop yields, and crime and conflict are sensitive to weather variation and therefore likely affected by changing climate patterns (*Carleton et al., 2022, Rode et al., 2021, Hsiang and Burke, 2014, Park et al., 2021, Moore et al., 2017*). Current estimates place the cost of one ton of CO_2 emissions at $200 per ton, with a possibility of much higher values (*EPA, 2023, Bilal and Känzig, 2026, Moore et al., 2024*).

This paper highlights an additional and as yet unquantified channel by which climate change imposes costs on society: the very possibility that the climate *might* be changing lowers the information content in the historic weather record and raises costs for actors managing weather risks. These costs arise because climate – a probability distribution over weather outcomes – is never observed directly. Instead the climate must be inferred, most commonly through observations of local weather. If the climate is not changing then a long enough weather record will precisely identify the current climate distribution. If the climate may be changing however, then older weather is potentially less informative about the

current climate state, leaving actors less confident about the climate distribution they face, raising the costs of managing weather risks.

These ambiguity-related costs will be particularly pronounced in the tails of the climate distribution for two reasons. Firstly, extreme events are, by definition, rare in the historic record. Even a relatively long weather record of 100 years contains, in expectation, one 1-in-100 year event and two 1-in-50 events. Actors therefore already face significant ambiguity in estimating the tail of the climate distribution. The loss of information associated with climate change would be expected to have a much larger relative effect in the tails of the distribution compared to the more frequently-observed center.

Secondly, very rare events tend to be the most costly. Societies are typically able to accommodate commonly occurring weather variation with minimal disruption. More infrequent events, however, can begin to exceed natural, engineered or social tolerances, leading to rapidly growing costs for increasingly rare events. Steeply non-linear damages will amplify the impact of elevated ambiguity in the tail of the climate distribution, producing even larger relative effects on the tail of the loss distribution than on the weather hazard itself.

This loss of confidence in the tails of the climate distribution has broad implications across geographies and economic sectors for actors seeking to manage weather risks. In this paper we quantify a particular set of costs related to the insurance of catastrophic risks but the cost implications are much more general. For instance, infrastructure design standards are typically based on weather return intervals such as a 1-in-100 or 1-in-200 year event (*Milly et al., 2008*). Ambiguity over exactly what constitutes such an event means infrastructure will, all else equal, need to be "over built" to maintain the same design tolerance relative to a world in which the climate distribution is known precisely. More generally, any actor able to undertake costs to protect themselves against downside weather risk will face higher costs under a more ambiguous climate.

Importantly, these ambiguity-related costs are additional to the actual costs and benefits of altered weather patterns due to climate change. They arise through the possibility of a moving climate distribution and the attendant loss of confidence in the quantification of weather risks. While the direct impacts of climate change could, in principle, be either positive or negative, these effects are unambiguously negative. Moreover, because these effects operate through a shift in inference, they can arise far more abruptly than direct climate impacts. The mechanism we identify here has the potential to generate sudden, Minsky-like shocks as actors re-evaluate historic weather patterns, despite the fact that climate change itself is a much more gradual process.

Here we illustrate how ambiguity-related costs arise from the combination of long-tailed weather variables, a potentially-changing climate distribution, and non-linear damage functions, using the case study of urban flooding in the United States. Flooding is the most widespread and costly natural disaster in the U.S., accounting for $8 billion in losses in 2024 (*FEMA, 2025*). Warmer air can hold more moisture, meaning climate change is likely to intensify extreme rainfall, raising flood risks (*Trenberth et al., 2003, Seneviratne et al., 2021*).

The paper has four main sections:

1. Using 1970-2024 time series of daily maximum rainfall for 151 US cities we estimate the 2024 distribution under two Bayesian models – one with time-constant parameters simulating a learner confident that the climate is unchanging and one with time-varying parameters simulating a learner who believes the climate may have changed over the historic period.

2. Using data on all policies and claims under the National Flood Insurance Program (NFIP) since 2001, we estimate city-specific damage functions relating annual rainfall maxima with flood losses.
3. Combining 1 and 2 gives us flood loss distributions under two alternate learning models, one in which the climate could be assumed to be unchanging and one where it is allowed to be time-varying.
4. We simulate the performance of portfolios of policies in 111 cities across the US at different levels of spatial diversification, accounting for correlations in extreme rainfall patterns across space, and estimate the increased cost of capital required to maintain a 1% chance of insolvency under a potentially-changing climate.

This paper contributes to three main groups of literature. Firstly, it adds to our understanding of the costs of climate change. A rich literature has developed in the last decade improving the empirical quantification of climate change costs using either a 'bottom-up" assessment of impacts and adaptation in each economic sector or "top-down" reduced-form regressions of GDP on weather variables (*Rennert et al., 2022, Rode et al., 2021, Carleton et al., 2022, Nath et al., 2024*). These approaches have in common a goal of quantifying the direct costs of changing weather patterns on outcomes of economic import such as productivity, capital, or mortality risk. The costs we describe here accrue in addition to these direct effects and arise from additional uncertainty and the accompanying undiversifiable risk that climate change brings. Costs associated with managing this risk are potentially widespread but, to date, completely unquantified. They constitute a broad, missing piece of our understanding of climate impacts that this paper begins to address.

Secondly this paper contributes to a rich literature on the implications of uncertainty and ambiguity for climate policy. These papers highlight the profound scientific uncertainty around climate change and the important role this plays in shaping optimal abatement policy, typically using integrated climate-economy models such as DICE. Effects investigated in this literature include the role of risk preferences, ambiguity aversion, scientific uncertainty over climate sensitivity, and stochastic "tipping points" in the climate system (*Lemoine and Traeger, 2016, Rudik, 2020, Hope, 2015, Cai and Lontzek, 2019, van den Bremer and van der Ploeg, 2021*). Our setting is distinct for a number of reasons. For instance, in contrast to these prior studies, we examine uncertainty-related climate costs that can arise even in the absence of ambiguity- or risk-aversion. In our setting even risk-neutral actors can experience ambiguity-related costs through the combination of shifts in the tail of right-skewed weather variables (raising expected losses) as well as institutional factors (in our case capital market frictions and regulatory solvency requirements) that require actors to respond to shifting tail risks. Moreover, in contrast to previous work, we focus on "climate takers" – the many households and businesses affected by climate change with little to any direct control over how it unfolds – not the "climate makers" directing global mitigation policy in integrated climate-economy models, with distinct policy implications.

Finally, this work contributes to understanding of recent instability in property insurance markets in the US. Insurers have seen persistent net-negative profits since the 2010s in many states while consumers have experienced premium costs outpacing inflation and lack of availability in some areas (*Fliegelman, 2023, Koller, 2024*). Existing work has linked this volatility to natural hazard risk, showing that rising premiums are concentrated in regions highly-exposed to wildfire and tropical storms, and has illustrated the important role of rising reinsurance costs (*Keys and Mulder, 2024, Boomhower et al., 2024*). This paper highlights the fundamental role that climate change might be playing, beyond

the direct losses from specific extreme events that may or may not be attributable to anthropogenic forcing (*Davenport et al., 2021, Brown et al., 2023*). We model a sudden loss of confidence in the information used to assess weather-related risks in the insurance sector associated with recognition of a shifting climate state. The consequences of this reassessment are substantial and are concentrated in the extreme tail of the climate distribution, the region that is most difficult and most expensive to underwrite. The effects of this information shock would be rapid increases in reinsurance costs, pull back from underwriting in regions with concentrated natural hazard risk, and growing insolvency risk with major events, all consistent with recent developments in the US property insurance market.

The paper proceeds as follows; Section 2 describes implementation of two Bayesian learning procedures on 55 years of maximum rainfall data for 151 cities across the US. Section 3 describes the estimation of city-specific flood-loss functions using the universe of National Flood Insurance Program (NFIP) claim and loss data. Section 4 combines the results from Sections 2 and 3 to develop posterior loss exceedance curves under the time-constant and time-varying learning models. Finally Section 5 simulates the financial performance of policy portfolios with different levels of geographic diversification.

2 Extreme Rainfall Under a Constant vs Time-Varying Climate

Intensification of rainfall extremes is a direct consequence of anthropogenic warming. Simply put, a warmer atmosphere can hold more moisture, which can be released catastrophically in periods of very intense rainfall[1]. These events can be particularly consequential in urban areas both because of the concentration of people and property in harms way, and because impervious surfaces in urban areas prevent infiltration of moisture into the ground. Intense rainfall extremes can overwhelm drainage infrastructure leading to dangerous and damaging flood conditions.

We compile daily rainfall data for 151 cities across the US for 1970 - 2024 from the Global Historical Climatological Network Daily dataset and extract a 55 year time series of daily maximum rainfall for each city (*Menne et al., 2012b, Menne et al., 2012a*). Figure 1 shows the location and average extreme rainfall climatology for all the cities, with detailed descriptive statistics in Appendix A.

The extreme value theorem connects the tail properties of a distribution to the asymptotic behavior of sample maxima drawn from that distribution. In particular, maxima from a broad family of distributions will converge to the Generalized Extreme Value (GEV) distribution, a family that encompasses the Gumbel, Frechet and Weibull distributions. The GEV is described using a location, scale, and shape parameters (μ, σ, ξ), which depend on the parameters of the underlying population distribution as well as the sample size, n.

In a recent paper, Müller and Watson describe a Bayesian procedure for estimating a time-varying path for GEV parameters from a time-series of sample maxima, distinguishing between changes due to shifts in the underlying distribution and a growing sample size (*Müller and Watson, 2024*). The procedure allows parameters to evolve in a random walk, simulating the learning process for an observer unsure whether the underlying distribution can be assumed to be stationary over the time-series. This

[1] Although this thermodynamic effect of climate change is unambiguous in direction, climate change can cause local rainfall extremes to either increase or decrease. If rainfall extremes in a region are associated with particular atmospheric dynamic processes (e.g. atmospheric rivers or cyclones), then climate change could decrease extreme rainfall intensity by altering these dynamic patterns. The net effect of climate change on extreme rainfall in a given location depends on the net effect of the thermodynamic and dynamic effects.

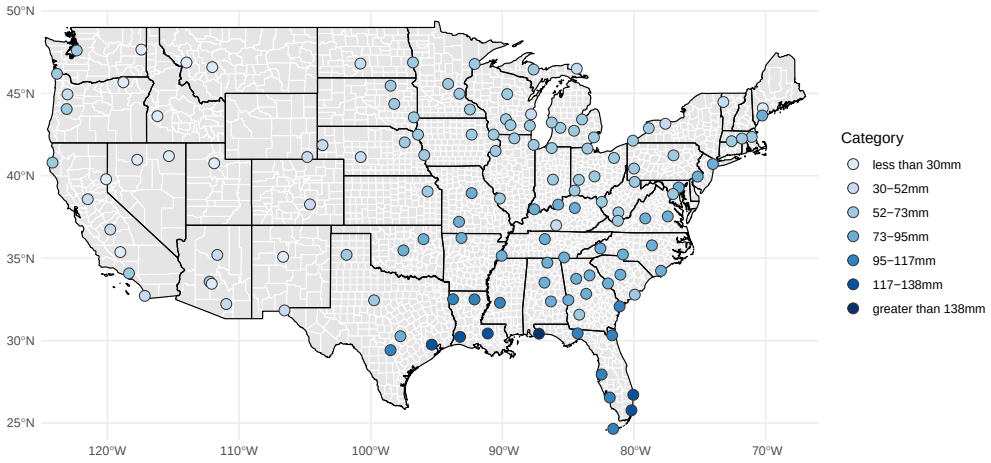


Figure 1: Location of 151 cities included in analysis, together with their average annual maximum daily rainfall, 1970-2024

time-varying model can be contrasted with a null, time-constant model, which restricts the estimated GEV parameters to constant values, simulating an observer confident the underlying distribution is not time-evolving. Further details on the functional form and priors are given in Appendix B.

We apply both time-varying and time-constant Bayesian models to the time-series of rainfall maxima for each of the 151 cities (Figure 2). Time series for eight illustrative mid-size cities from regions across the US are shown above, together with the mean and 99th percentile of the Bayesian posteriors under the time-varying and time-constant models. These show the large destabilizing effect of shifting from a time-constant model to a time-varying model, particularly on the tails of the posterior. Despite the fact that the data-series are identical in both inference models, inference that allows for time-evolving GEV parameters results in wider tailed-distributions. For these Bayesian learners, a single very large outlier in the distribution (e.g. Houston) or a series of moderately large events (e.g. Raleigh) could be evidence of a shifting rainfall distribution, with the potential to deliver much larger extreme events than are observed to date in the historic record. In contrast, a learner confident that the data reflect a single, time-constant distribution will still shift their beliefs in response to a large event. But because they "know" all data in the series come from one unchanging distribution, they are better able to attribute that event to an unlucky draw, rather than a fundamentally altered climate state, resulting in a smaller posterior shift and thinner right tail.

The lower panels in Figure 2 show summary statistics from the 2024 posterior distributions for all cities. They show the patterns from the 8 illustrative cities generalize to the full set of cities. The lower left panel shows a modest upward shift in the posterior mean. 111 of the 151 cities have a posterior mean in the time-varying model that is larger than in the time-constant model with a population-weighted average increase of 4.5%. The lower right panel shows the far more pronounced difference in the tail of the distribution. In almost all cities (89%), the 99th percentile is larger in the time-varying than the time-constant model, with a population-weighted change of 27%. In four cities (Houston, Pensacoloa, Richmond, and Scottsbluff) the posterior 99th percentile more than doubles from the time-constant to the time-varying learning model.

Importantly, substantial shifts in the tail of the posterior distribution can come about even in the absence of overwhelming statistical evidence of time-varying parameters. Muller and Watson (*Müller and Watson, 2024*) implement a Nyblom test for GEV parameter instability, against the null of constant GEV parameters. Applying this test to each of our cities, we reject the null of parameter stability for only 20 cities at the 95% confidence level, 8 of which would be expected due to multiple hypothesis tests. Standard scientific approaches to statistical inference then would suggest a constant parameter model. But the plausibility of this model in real-world decision contexts, given knowledge of climate change and its connection to rainfall extremes, is questionable. Thus, the existence of climate change, even absent a clear statistical "fingerprint" in local weather records, could drive actors to adjust their interpretation of past weather patterns, with substantial increases in assessments of tail risk.

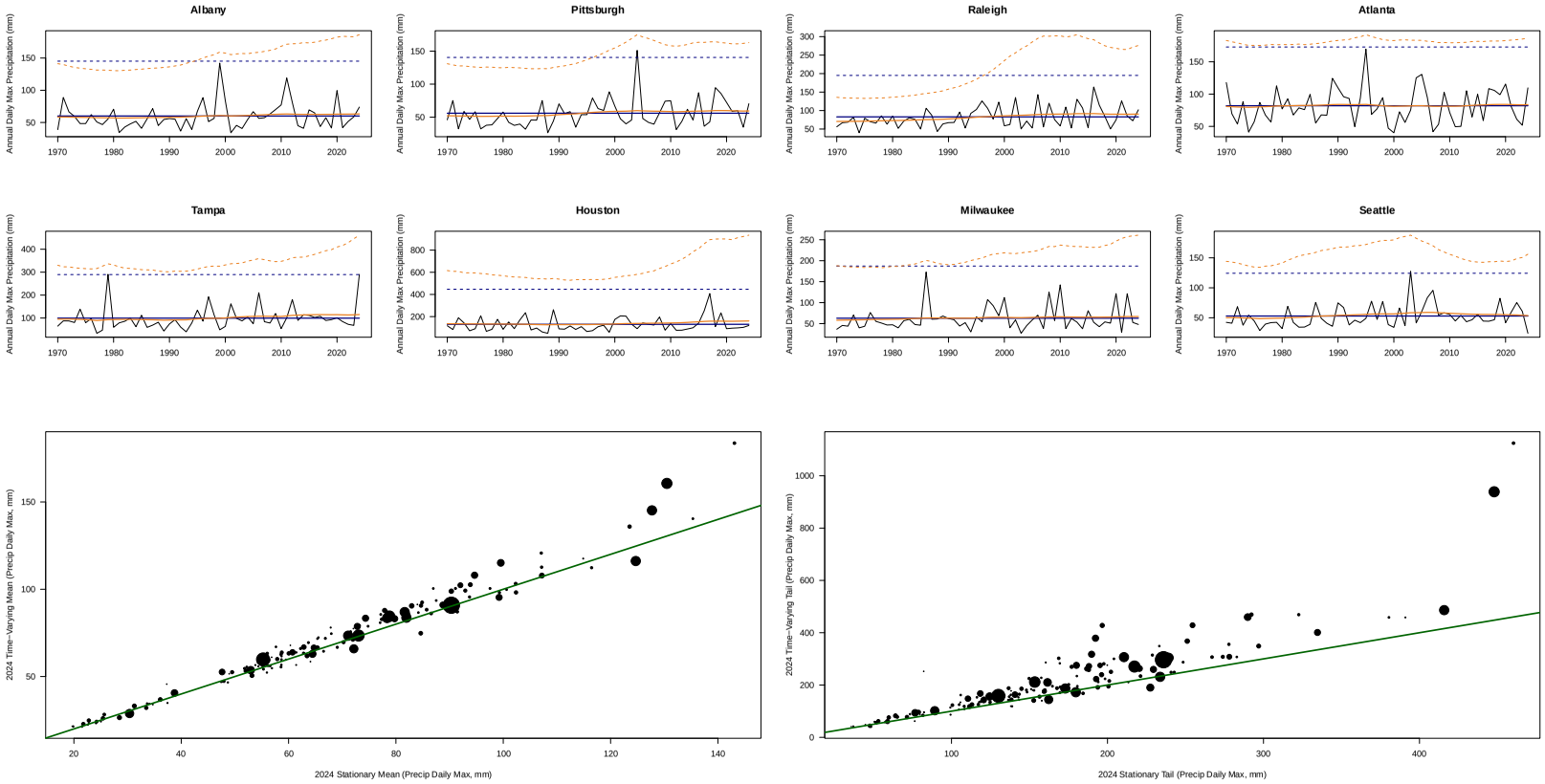


Figure 2: Annual daily rainfall maxima for eight example cities with mean (solid) and 99th percentile (dashed) of the Bayesian posterior in the time-varying (orange) and time-constant (purple) model (Upper). Comparisons of mean (left) and 99th percentile (right) in 2024 for all 164 cities (lower). Size of point is scaled based on population in each city in 2024. Posterior rainfall distributions are based on 6 million draws, 1500 rainfall draws for each of 4000 samples from the posterior parameter space for each learning model.

3 Costs Increase Steeply with Rainfall Intensity in Most Cities

Weather extremes are consequential because of the deaths and property loss they bring about. The weather is always changing and societies have evolved in the presence of this variation, developing technologies, infrastructure and social systems to limit costs of regularly-experienced variation. Rare weather events, however, may often exceed the tolerances of these systems, leading to steeply-increasing costs with larger extremes. These non-linear damage functions will amplify the social and economic consequences of shifts in the tail of the climate distribution. In this section we develop city-specific flood loss functions using NFIP data.

3.1 City-Specific Flood Damage Functions

3.1.1 Data

Our primary dependent variable is the expected flood loss per policy, as a fraction of building replacement cost. Data comes from Open FEMA's NFIP redacted policy and claims datasets (*Federal Emergency Management Agency (FEMA), 2026a, Federal Emergency Management Agency (FEMA), 2026b*). The Federal NFIP provides essentially all flood insurance coverage in the United States. Rates of flood insurance nationally are very low, with coverage highly concentrated in designated flood hazard areas. The claims data include the universe of NFIP claims since 1970. Our policy data include the universe of NFIP policies since 2001[2]. Flood claims and policies are aggregated to the year level and matched to cities based on zip codes using the Department of Housing and Urban Development zip code to CBSA crosswalk table[3].

Our independent variable is the time series of annual daily maximum rainfall in each city, for compatibility with the posterior distributions estimated in Section 2, with data obtained from the Global Historical Climatological Network Daily dataset. Flooding is broadly categorized into three types: 1) pluvial, when rainfall leads to inundation; 2) fluvial, when rivers overflow their banks, and 3) coastal, when storm surge pushes seawater inland. The maximum rainfall measure that we use as our independent variable is most closely associated with pluvial flooding, but a well-recognized feature of extreme rainfall events is that they can also lead to fluvial and coastal flooding (*NOAA, nd*). For instance, intense rainfall in the Gulf region is associated with tropical cyclones that also create storm surge. In general, we do not add controls for drivers of flooding other than extreme rainfall (such as river stage and tide height for coastal cities)[4]. Our estimated responses will therefore capture riverine and coastal flooding, in addition to pluvial flooding, to the extent those flood events are correlated with regional rainfall extremes.

3.1.2 Model

We model the expected flood damage as a fraction of replacement cost for each city as function of annual maximum daily rainfall. Fitting separate models for each city captures the city-specific hydrology, development patterns, drainage and flood defenses that would be expected to mediate the

[2]Open FEMA data includes policies since 2009. We supplement these data with effectively identical proprietary data on policies dating back to 2001 (*Collier et al., 2022*).

[3]We use building replacement cost as the denominator, rather than policy coverage, because the $250,000 coverage cap in the NFIP has become increasingly binding over time. In principle this could create spurious trends in the fraction of coverage damaged over time. Normalizing by the building replacement cost removes this concern and also makes results more applicable to the private insurance markets where buildings are typically insured at their replacement cost.

[4]The one exception is New York City, where Hurricane Sandy in 2012 caused massive flooding from a huge storm surge. Controlling for tide height in New York captures this outlier event and substantially improves precision of the estimated rainfall response.

effect of rainfall on flooding and losses. Since flood claims are rare in the data (i.e. there is a very large probability mass at zero), we model expected losses using a hurdle model that separately captures 1) the probability of any loss in a year and 2) the severity of damages conditional on a loss.

For each city, the first stage models the fraction of policies in zip code z in year t that file a claim (p_{zt}) using a binomial logit:

$$logit(p_{zt}) = \alpha_1 + \beta_1 R_t + \epsilon_{zt}$$

where α_1 are city fixed effects, R_t is the annual maximum of daily rainfall in year t and ϵ_{zt} is an error term.

In the second stage, the expected loss from claim c in zip code z in year t, as a fraction of building replacement cost (μ_{czt}), is modeled using a fractional logit model (*Papke and Wooldridge, 1996*):

$$logit(\mu_{czt}) = \alpha_2 + \beta_2 R_t + \nu_{czt}$$

The regressions are weighted by the number of flood insurance policies in a location, calculated as the fraction of residential addresses in each zip code in the CBSA multiplied by the number of flood policies in that zip code.

Our estimates are the average response of insured losses within a city to extreme rainfall, not overall flood damages. If flood coverage is concentrated within parts of a city that are more vulnerable to flooding, our estimates will reflect that differential vulnerability, not a city-wide average of all properties. We omit from our analysis six small cities, which each have fewer than 10 total claims over the period. Standard errors in both models are two-way clustered at the year and zip code level, although we do not propagate uncertainties in damage estimates forward in the analysis.

3.1.3 Estimated Loss Functions

Expected loss per policy as a function of any given annual maximum rainfall level R is the estimated probability of any claim multiplied by the fraction lost conditional on a claim:

$$E[L \mid R] = p_{zt} * \mu_{czt} = \left[\frac{\exp\left(\hat{\alpha}_1 + \hat{\beta}_1 R\right)}{1 + \exp\left(\hat{\alpha}_1 + \hat{\beta}_1 R\right)}\right]\left[\frac{\exp\left(\hat{\alpha}_2 + \hat{\beta}_2 R\right)}{1 + \exp\left(\hat{\alpha}_2 + \hat{\beta}_2 R\right)}\right] \quad (1)$$

The shape of the loss function depends on the magnitude and sign of both the intercept and rainfall coefficient terms in both models and can not be easily intuited directly from regression coefficients. We instead plot the response curves graphically out to 1.25 times the maximum observed daily rainfall over the 1970-2024 period for each city.

Figure 3 shows damage functions for the eight illustrative cities also shown in Figure 2, along with the 1970-2024 histogram of annual maximum daily rainfall. Damage functions for these cities are generally plausible in terms of being upward sloping and convex. Losses are minimal in the center of the climate distribution but grow rapidly in the right tail at rarer and more extreme rainfall events. Although exhibiting qualitatively similar shapes, the size of the response differs by orders of magnitudes between

cities, from a maximum expected loss of less than 2.5% over the simulated range in Raleigh to over 25% in Tampa.

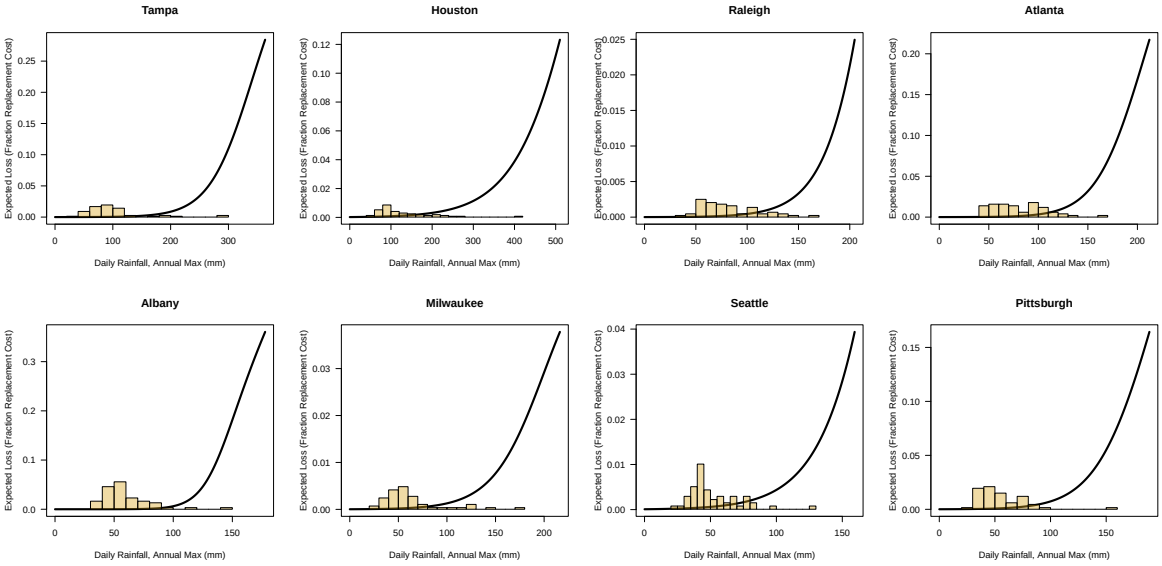


Figure 3: Damage functions for eight illustrative mid-size cities relating annual maximum daily rainfall to the per policy expected loss. Histograms show the distribution of maximum daily rainfall 1970 to 2024. Damage functions are plotted out to 1.25 times the maximum daily rainfall in the 1970-2024 period.

Not all damage functions are as reasonable as those shown in Figure 3. Rather than retain noncredible damage functions we filter cities based on a loose criteria that the estimated function not be downward sloping over the historical rainfall distribution, which drops 7 cities leaving a remaining 111 in the analysis. Appendix D plots damage functions for all these 111 cities.

Note that our selection procedure retains cities for which the estimated response is very small and not indistinguishable from zero, as long as the central estimate is not downward sloping. A number of cities fall into this group (Tulsa, Lansing and Colorado Springs are some examples) and retaining them in the analysis is important. For reasons potentially related to drainage, topography, flood defenses or development patterns, these cities do not exhibit strongly correlated risks, at least as related to extreme rainfall-driven flooding. They thus provide potential diversification benefits to insurers, an element we would miss if limiting our analysis only to cities with large, precisely estimated rainfall responses.

4 Non-Linear Loss Functions Amplify Tail Ambiguity

We propagate our extreme rainfall posteriors through these loss functions to develop damage distributions under both the time-constant and time-varying learning models. The largely upward-sloping and convex loss functions amplify changes in the tail of the posterior climate distributions, driving even larger relative movement in the economically-relevant loss distribution. Figure 4 gives the 2024 loss exceedance curves (the probability of a given loss level being exceeded) for the eight illustrative cities also shown in Figures 2 and 3. For all cities, the loss distribution using time-varying climate parameters is to the right of the distribution assuming a time-constant climate, meaning the probability of exceeding any given loss level has increased.

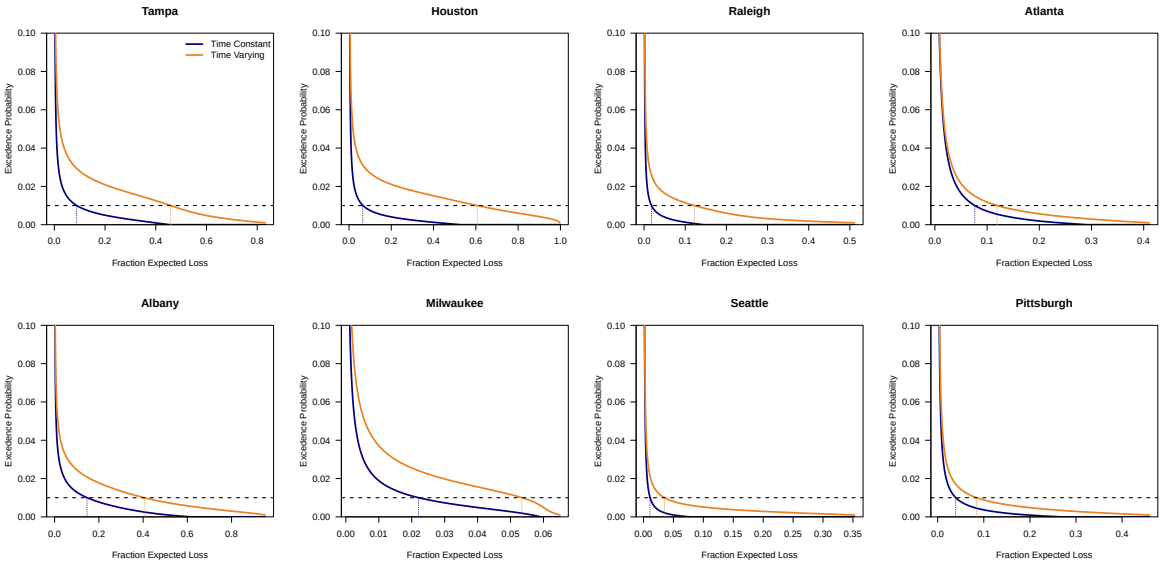


Figure 4: 2024 loss exceedance curves for eight illustrative cities under learning models with time-constant (blue) or time-varying (orange) climate parameters. Black dashed lines give the 1% exceedance probabilities. Loss distributions are based on 6 million draws - 1500 rainfall draws for each of 4000 samples from the posterior parameter space for each learning model. X-axis gives the loss measured as average per-policy loss as a fraction of building replacement cost.

Dashed lines in Figure 4 highlight the 1% exceedance level, significant because this standard (or in some cases a higher 0.5% standard) is used for financial solvency regulation of insurance markets (*National Association of Insurance Commissioners, 2024*). Insurance regulators specify some risk tolerance (e.g., that the likelihood of insurer insolvency should be at most 1%), and the exceedance curve provides the size of the loss at this probability, called the "probable maximum loss" (PML)[5]. Insurers must demonstrate an ability to pay claims up to this loss level to fulfill regulatory capital requirements. Therefore, increases in this tail loss level have direct effects on insurer operating costs as they must maintain access to sufficient capital (either through their own equity holdings or contracting with reinsurers) to pay claims for an event of this magnitude. In all cities shown in Figure 4 this financial management standard shifts higher, consistent with a widening of the right tail of the loss distribution. In some cases (e.g. Seattle) this increase is quite modest. In some other cases (e.g. Milwaukee) the relative increase is quite large (in this case more than doubling from 2.2% of the building replacement cost to 5.3%) but the absolute magnitude remains reasonable and likely quite manageable for an insurer. In more extreme cases (e.g. Houston and Tampa) where large shifts in the climate posterior combine with steep damage functions, the change in the 1% loss level is significant in both absolute and relative terms. In Tampa, for instance, it increases from just under 9% to over 45% while in Houston it increases by almost a factor of 10 from 6.6% to 60%.

Figure 5 plots summary statistics from the loss distribution for all 111 cities retained in the analysis, showing the general insights from Figure 4 carry over when considering the full collection of cities. The horizontal axis plots values from the time-constant model, and the vertical axis from the time-varying model. The solid-line reflects a 1-to-1 relationship; estimates would fall on this line if the time-constant and time-varying models resulted in the same values. Losses are almost universally higher under the time-varying compared to the time-constant model in both the mean (86% of cities) and tail (89%) of

[5]Banking regulation applies the same concept but refers to PML as "value at risk."

the distribution. Moreover, because of the amplifying effect of convex loss functions, on average the relative magnitude of the increase is much larger than for the climate distribution itself. Population-weighted mean losses increase by a factor of 2.2 (from 0.17% to 0.37%), compared to a 27% change in the inferred mean climate state. Tail losses increase by a factor of 4.4 (from 2.2% to 10.0%), more than double the increase in the tail of the climate distribution.

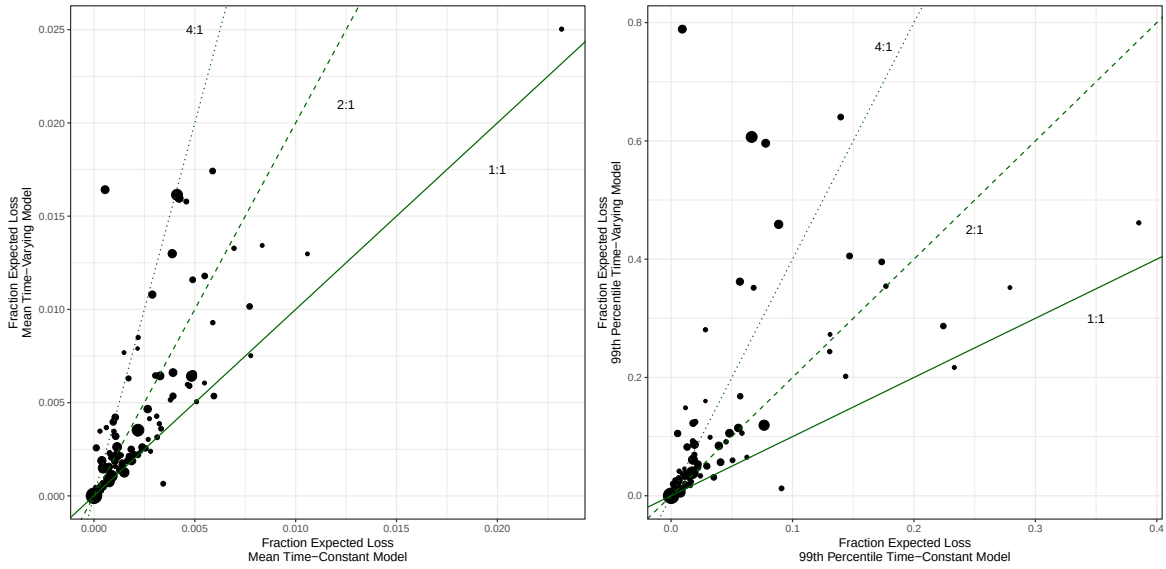


Figure 5: Summary statistics for the 2024 loss distribution for all cities under time constant (x-axis) and time-varying (y-axis) learning models. Mean (left) and 99th percentile (right) with the 1:1, 2:1, and 4:1 lines. Size of points is scaled by 2024 population.

This widening of the loss distribution tail potentially constitutes a very meaningful shock in the industry's understanding of catastrophic risk. Expected losses on average more than double, creating real costs that would, in principle, ultimately fall to homeowners in the form of higher insurance premiums.

Even larger growth in tail risk creates further challenges. Financing losses up to 10% of underwriting is a very different proposition to financing losses of 2%. To meet the same 1% financial solvency standard under this new understanding of current climate risk, insurers would either need access to substantially more capital, raising costs, or to restrict their underwriting in areas with most concentrated risk. Alternatively, insurers might operate at a lower financial solvency standard if allowed by regulators, effectively moving risks onto state guaranty funds and asset owners.

5 Evaluating the Potential of Geographic Diversification

The analysis in Section 4 focused on the individual city level. One question is whether an insurer could effectively mitigate the additional tail risks arising from a more ambiguous climate through a geographically-diversified portfolio of cities. To investigate this question we simulate performance of a series of portfolios aggregating from the city to state to regional to national scale, simulating insurance companies operating across a range of levels of geographic diversification.

5.1 Simulating Policy Portfolios

The joint distribution of extreme rainfall across all 111 cities is simulated using a Gaussian copula that separates the specification of marginal distributions from the dependence structure across cities. Let $\mathbf{Y} = (Y_1, \ldots, Y_L)$ denote the vector of extreme rainfall realizations across L locations. Each city is assumed to follow a generalized extreme value (GEV) distribution,

$$Y_i \sim \text{GEV}(\mu_i, \sigma_i, \xi_i),$$

with GEV parameters derived from the Bayesian learning models under either time-varying or time-constant parameters, as described in Section 2. While this specification captures the marginal distribution of extremes for each city, it does not impose any cross-sectional dependence. Because large-scale weather events may affect multiple cities simultaneously, incorporating dependence across locations is essential to assess the performance of geographically-diversified portfolios.

In the Gaussian copula, dependence across cities is captured using draws from a latent multivariate normal distribution

$$\mathbf{Z} = (Z_1, \ldots, Z_L) \sim \mathcal{N}(0, \hat{\Sigma}),$$

where $\hat{\Sigma}$ is the empirical covariance matrix estimated from the 1970-2024 annual max daily rainfall across the 111 cities. Long-term climate trends in each city are removed using a Hodrick-Prescott (HP) filter with smoothing parameter $\lambda = 100$. This ensures the correlation matrix reflects regional synchronization in extreme rainfall rather than common drift in the distributional mean due to climate change. The estimated $\hat{\Sigma}$ is shown in Appendix E. It shows some inter-regional correlated rainfall patterns (for instance in the northeast and northwest) where nearby cities tend to see the most extreme rainfall events in the same year. However, geographically-distant cities within the U.S. have only weakly correlated rainfall extremes, suggesting the potential for diversification benefits at larger scales.

The latent vector $\mathbf{Z}$ encodes the correlation structure across locations through the $\hat{\Sigma}$ matrix but the normally-distributed $\mathbf{Z}$ needs to be transformed into GEV-distributed values consistent with the marginal rainfall distributions in each city. This is accomplished via analytic formulas for both the normal CDF and the inverse GEV CDF, effectively mapping the quantiles from the latent variable Z_i to the marginal distributions, Y_i. Specifically, each city-level draw Z_i is transformed into a uniform variable using the standard normal CDF,

$$U_i = \Phi(Z_i),$$

which produces variables that are marginally distributed as Uniform$(0, 1)$ while preserving the dependence structure across cities implied by $\hat{\Sigma}$. These are mapped back into the city-level GEV distribution using the inverse GEV cumulative distribution function,

$$Y_i = F^{-1}_{\text{GEV}_i}(U_i).$$

This procedure guarantees that each marginal Y_i follows its estimated GEV distribution, while cross-location dependence arises from the Gaussian copula defined in the latent space. The resulting simulations therefore combine empirically grounded marginal extreme-value behavior with a dependence structure consistent with the observed covariance across locations, capturing potential cross-city correlation in extreme rainfall conditions.

To simulate portfolio-level extreme rainfall risks under both time-constant and time-varying Bayesian models, we combine the copula procedure described above with the posterior GEV parameter distributions for each city described in Section 2. Losses from a given portfolio with city weights w_i under parameter draw p from Bayesian posterior m and copula draw $\mathbf{Z}$ is

$$L_{pmZ} = \Sigma_i w_i D_i(F^{-1}_{\text{GEV}_{pmi}}(\Phi(Z_i))$$

where D_i is the city-specific damage function from Section 3.1, $F^{-1}_{\text{GEV}_{pmi}}$ is the inverse GEV distribution given by a draw from the city and model-specific posterior distribution and Z_i is the city i component of the joint copula draw $\mathbf{Z}$. We sample systemic risk using 2000 draws from the copula and city level idiosyncratic risk using 4000 draws from the posterior for each copula draw, giving 8 million samples of the loss distribution for each city under each Bayesian model.

Portfolios are defined at the state level (our 111 cities span 40 of the contiguous states), at the regional level (9 geographic regions based on the NOAA climate regions (*NOAA National Centers for Environmental Information, 2026*)), and nationally across all 111 cities. Portfolio weights are based on the distribution of NFIP policies in 2024. There is strong selection into NFIP coverage based on pre-existing flood risk. For instance, 79% of policies in 2024 in our 111 cities were in the South or Southeast regions highly exposed to hurricanes. Portfolios defined based on NFIP coverage will therefore be more exposed to catastrophic risk than population- or asset-weighted portfolios, capturing the selection processes operating when insurance coverage is not universally required, as is the case with flood risk in the US. Alternative portfolios based on population or property distributions, more characteristic of required peril coverage, will be investigated in future work.

5.2 Ambiguity Costs of Climate Change are Substantial and Not Geographically-Diversifiable

Exceedance curves for the fully-diversified national portfolio under both learning models are shown in Figure 6. The tail of the loss distribution shows substantial thickening, with the PML increasing by more than a factor of 4 from 4.10% loss per policy to 18.09%. Mean losses also increase by a factor of 2.5 from 0.34% to 0.85%. From an insurer perspective, changes in expected loss and tail risk are distinct: the former can be passed on to policy-holders in the form of higher premiums, while the latter raises capital requirements and the cost of supplying insurance. The right panel of Figure 6 shows widening in the tail of the loss distribution even after controlling for increase in the expected loss, with the PML almost doubling from 11.9 times the expected loss to 21.3 times.

Table 1 gives summary statistics from the national and 9 regional portfolio loss distributions under both learning models. In almost all cases, the mean and PML of these geographically-diversified portfolios increase under time-varying climate parameters, with larger relative increases in the tail than in the mean, consistent with findings from the city level (i.e. Figure 5). Table 1 also shows the substantial regional variation in both the level of risk and the relative increase under a time-varying climate. Both mean and catastrophic risk are highest in the hurricane-exposed South and Southeast regions, though there is also substantial risk in central regions (Ohio Valley and Upper Midwest), an area that has seen widespread flooding in recent years.

The benefits of diversification can be assessed by considering how the tail of the loss distribution changes as the same risk is integrated into portfolios at different levels of spatial aggregation. In 2024, the policy data includes $586 billion in total insured value across the 111 cities in our dataset.

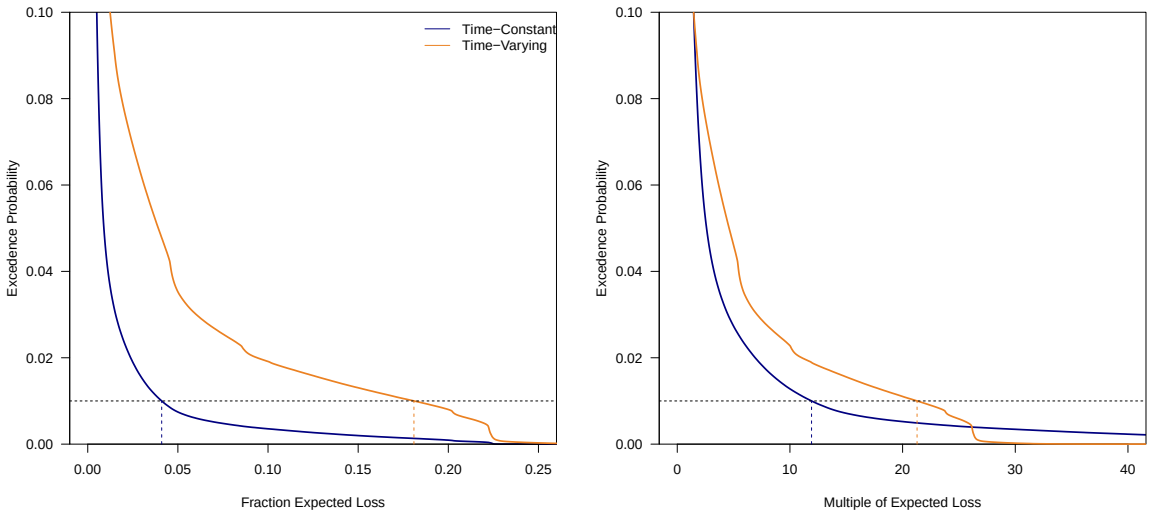


Figure 6: Exceedance curves for national portfolio of flood policies across 111 cities under time-constant (blue) and time-varying (orange) climate parameters. Dotted line shows the 1% PML. Curves are plotted both as the expected loss per policy as a fraction of replacement cost (left) and normalized by expected value of the loss distribution (right).

Figure 7 simulates how the PML for this bundle of policies changes as policies are aggregated across different levels of spatial aggregation, from city to national[6]. We find the expected benefits of spatial diversification, with PML in the city-level aggregation (i.e. assuming each city is insured by an insurer operating only in that city) 13% larger than than in the national portfolio under time-constant climate parameters ($27.2 vs $24.1 billion).

However, Figure 7 also show the modest benefits of geographic diversification compared to the large and systemic information shock caused by climate change. PML values under time-varying climate parameters are consistently 4-5 times larger than under time-constant climate parameters at all levels of aggregation. PML under the most diversified national policy under time-varying parameters is still 3.9 times larger than the least diversified portfolios under time-constant climate. Because the climate change information shock is systemic, affecting all regions simultaneously, it cannot be substantively reduced via spatial diversification. Moreover, the same information shock extends to other countries and to other weather risks (wind, wildfire, hail), meaning the potential benefits from either cross-peril or cross-country diversification in offsetting these costs is also likely limited.

Ambiguity in this setting translates directly into higher costs because financial solvency regulations require insurers to hold capital sufficient to pay claims up to the PML (*National Association of Insurance Commissioners, 2024*). In our setting, a national-scale insurer covering the same bundle of properties as the NFIP sees climate-change related ambiguity increase the PML by $82 billion (from $24 to $106 billion), or 14% of the total insured value. Insurers can access this capital by issuing equity, paying a typical return of 10% to investors (*Aon, 2026, Swiss Re Institute, 2025*). Alternatively, insurers can transfer tranches of their catastrophic risk to reinsurers or to capital markets via insurance linked securities. In this case they pay a premium that is some multiple of the expected loss, with higher risk tiers (i.e. more unlikely events) commanding higher premiums relative to expected loss. Using

[6]In other words, the city-level aggregation sums the PML for each city (total NFIP coverage in each city multiplied by the 99th percentile loss per policy) while the state-level aggregation sums the PML across each state-level portfolio.

	Probable Maximum Loss		Mean	
Portfolio	Time Constant	Time Varying	Time Constant	Time Varying
National	**4.10**	**18.09**	**0.34**	**0.85**
NorthernRockiesPlains	0.38	0.56	0.22	0.23
South	8.15	48.46	0.55	1.62
OhioValley	2.83	11.68	0.28	0.58
Northeast	0.60	1.19	0.05	0.11
Southwest	0.02	0.03	0.01	0.01
Southeast	3.58	11.48	0.31	0.61
Northwest	1.63	3.86	0.18	0.31
UpperMidwest	2.98	4.70	0.27	0.42
West	0.19	3.24	0.03	0.16

Table 1: Probable Maximum Loss (99th Percentile) and mean of loss distributions for national and regional policy portfolios. Values are expected loss per policy as percent of building replacement cost.

an 8% cost of capital assuming a mix of equity and reinsurance implies increased capital costs of $6.6 billion per year. For comparison, total policy cost across all 111 cities is only $2.8 billion per year[7] and expected losses are either $2.0 or $5.0 billion under either the time-constant vs time-varying model.

6 Discussion and Conclusion

The presence of climate change destabilizes society's understanding of weather risks as past experience can no longer be assumed to constrain current climate exposure. Climate change reduces the information content in the historic weather record, with broad implications for any actor making weather-contingent decisions. These ambiguity-related costs will be most pronounced in the tail of the climate distribution (i.e. extreme events) for two reasons: firstly, these events are already poorly constrained in the historic record because they are rare by definition and, secondly, non-linear loss functions amplify the consequences of weather extremes, making uncertainty particularly costly. These costs accrue broadly but are challenging to quantify comprehensively because they depend sensitively on details of climate exposure, loss functions, and the costs of protective actions that are not systematically quantified for all regions, sectors, and weather risks.

Here we quantify ambiguity-driven climate change costs for a major sector, namely urban flood damages in the United States. We show how a loss of confidence in the stability of the climate distribution can change actors' interpretation of current weather risks, with effects rippling through the loss distribution and with implications for premiums as well as reinsurance and capital costs. These costs are quantitatively significant and can arise suddenly as actors shift their interpretation of historic data given the possibility of a changing climate. Although in practice US flood risks are covered through the public NFIP, these insights are almost certainly transferable to privately-insured perils such as wind, wildfire and hail.

One open question is the degree to which scientific modeling can substitute for historic weather data in constraining the climate distribution. For the last 30 years or so, catastrophic ("cat") modeling has served as an input into insurance against natural hazards, particularly hurricanes and earthquakes and increasingly wildfires (*Boomhower et al., 2024*). Cat models combine structural geophysical models, stochastic sampling of hazard event sets, and detailed data on property exposure and vulnerability to

[7] This includes the policy premiums, as well as various NFIP-specific charges such as the reserve fund assessment and federal policy fee. It also includes grandfathered subsidies in some areas that lower premium costs below what would be charged by a private insurer.

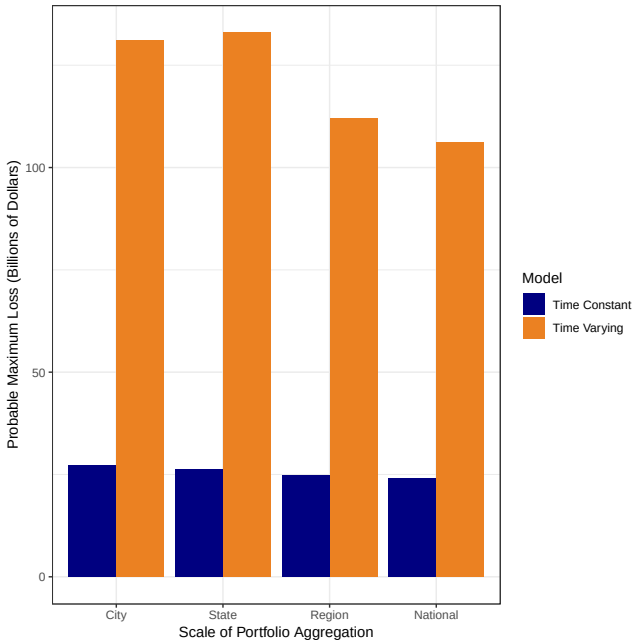


Figure 7: Probable maximum loss (99th percentile of loss distribution) for 2024 NFIP coverage in 111 US cities under different levels of spatial aggregation.

generate loss distributions used to price policies (*Guin et al., 2024*). Increasingly, cat modeling firms are seeking to explicitly account for anthropogenic climate change, for instance through linkages with General Circulation Models (GCMs) (*Guin et al., 2024*).

This modeling is unlikely to substantively offset the climate information shock we highlight here, for three reasons. Firstly, although GCMs have an excellent record of simulating the global temperature response to greenhouse gas emissions, these tools are not designed for risk-management applications (*Hausfather et al., 2020, Pitman et al., 2022, Fiedler et al., 2021*). The ability of GCMs to simulate the distributions of extreme events and their evolution under anthropogenic forcing is not clear and there are increasing discrepancies between model simulations of regional trends in risk-relevant weather variables and observations (*Simpson et al., 2025, Simpson et al., 2024, Sobel et al., 2023, Shaw and Stevens, 2025*). Secondly, cat models require calibration and validation against historical weather and loss data. Models integrating a non-stationary climate component will have more parameters and thus less degrees of freedom than models without anthropogenic forcing. In this sense, the general insight from this paper that climate change constitutes an information shock that reduces confidence in estimates of current weather risks carries over to the cat modeling space. Finally, although cat models are widely used in insurance applications, high costs make them inaccessible to the many other actors - households, firms, governments, and non profits - managing weather risk, leaving them fully exposed to the ambiguity described here.

Acknowledgments

Frances C. Moore acknowledges funding from National Science Foundation (award number 2446813). The authors have no competing interests to declare.

References

Aon, 2026. Aon (2026). Reinsurance market dynamics: January 2026 renewal. Market report, Aon plc.

Bilal and Känzig, 2026. Bilal, A. and Känzig, D. R. (2026). The macroeconomic impact of climate change: Global vs. local temperature. *Quarterly Journal of Economics*.

Boomhower et al., 2024. Boomhower, J., Fowlie, M., Gellman, J., and Plantinga, A. J. (2024). How are insurance markets adapting to climate change? risk selection and regulation in the market for homeowners insurance.

Brown et al., 2023. Brown, P. T., Hanley, H., Mahesh, A., Reed, C., Strenfel, S. J., Davis, S. J., Kochanski, A. K., and Clements, C. B. (2023). Climate warming increases extreme daily wildfire growth risk in california. *Nature*, 621(7980):760–766.

Cai and Lontzek, 2019. Cai, Y. and Lontzek, T. S. (2019). The social cost of carbon with economic and climate risks. *Journal of Political Economy*, 127:2684–2734.

Carleton et al., 2022. Carleton, T. A., Delgado, M., Greenstone, M., Houser, T., Hsiang, S. M., Hultgren, A., Jina, A., Kopp, R. E., McCusker, K., Nath, I., Rising, J., Rode, A., Seo, H. K., Simcock, J., Viaene, A., Yuan, J., and Zhang, A. T. (2022). Valuing the global mortality consequences of climate change accounting for adaptation costs and benefits. *Quarterly Journal of Economics*.

Collier et al., 2022. Collier, B. L., Schwartz, D., Kunreuther, H. C., and Michel-Kerjan, E. O. (2022). Insuring large stakes: A normative and descriptive analysis of households' flood insurance coverage. *Journal of Risk and Insurance*, 89(2):273–310.

Davenport et al., 2021. Davenport, F. V., Burke, M., and Diffenbaugh, N. S. (2021). Contribution of historical precipitation change to us flood damages. *Proceedings of the National Academy of Sciences of the United States of America*, 118.

EPA, 2023. EPA (2023). Epa report on the social cost of greenhouse gases: Estimates incorporating recent scientific advances. Technical report, Environmental Protection Agency.

Federal Emergency Management Agency (FEMA), 2026a. Federal Emergency Management Agency (FEMA) (2026a). Fima nfip redacted claims – v2. https://www.fema.gov/openfema-data-page/fima-nfip-redacted-claims-v2. OpenFEMA dataset. Accessed: 2026-01-25.

Federal Emergency Management Agency (FEMA), 2026b. Federal Emergency Management Agency (FEMA) (2026b). Fima nfip redacted policies – v2. https://www.fema.gov/openfema-data-page/fima-nfip-redacted-policies-v2. OpenFEMA dataset. Accessed: 2026-01-25.

FEMA, 2025. FEMA (2025). Know your risk: Cost of flooding.

Fiedler et al., 2021. Fiedler, T., Pitman, A. J., Mackenzie, K., Wood, N., Jakob, C., and Perkins-Kirkpatrick, S. E. (2021). Business risk and the emergence of climate analytics. *Nature Climate Change*, 11:87–94.

Fliegelman, 2023. Fliegelman (2023). Wind, fire, water, hail: What is going on in the property insurance market and why does it matter?

Guin et al., 2024. Guin, J., Towlinski-Ward, S., Jackson, C., Dodov, B., and Grenier, R. (2024). Insights into industrial catastrophe risk climate peril modelling, and cross-sector opportunities for progress. *Journal of Catastrophe Risk and Resilience*, 1.

Hausfather et al., 2020. Hausfather, Z., Drake, H. F., Abbott, T., and Schmidt, G. A. (2020). Evaluating the performance of past climate model projections. *Geophysical Research Letters*, 47.

Hope, 2015. Hope, C. (2015). The $10 trillion value of better information about the transient climate response. *Philosophical*
20140429.

Hsiang and Burke, 2014. Hsiang, S. M. and Burke, M. (2014). Climate, conflict, and social stability: what does the evidence say? *Climatic Change*, 123:39–55.

Keys and Mulder, 2024. Keys, B. J. and Mulder, P. (2024). Property insurance and disaster risk: New evidence from mortgage escrow data.

Koller, 2024. Koller, S. (2024). The insurance crisis continues to weigh on homeowners.

Lemoine and Traeger, 2016. Lemoine, D. and Traeger, C. P. (2016). Ambiguous tipping points. *Journal of Economic Behavior Organization*, 132:5–18.

Menne et al., 2012a. Menne, M. J., Durre, I., Korzeniewski, B., McNeill, S., Thomas, K., Yin, X., Anthony, S., Ray, R., Vose, R. S., Gleason, B. E., and Houston, T. G. (2012a). Global historical climatology network - daily (ghcn-daily), version 3. Accessed: YYYY-MM-DD.

Menne et al., 2012b. Menne, M. J., Durre, I., Vose, R. S., Gleason, B. E., and Houston, T. G. (2012b). An overview of the global historical climatology network-daily database. *Journal of Atmospheric and Oceanic Technology*, 29(7):897–910.

Milly et al., 2008. Milly, A. P. C. D., Betancourt, J., Falkenmark, M., Hirsch, R. M., Zbigniew, W., Lettenmaier, D. P., Stouffer, R. J., and Milly, P. C. D. (2008). Stationarity is dead : Stationarity whither water management ? *Science*, 319.

Moore et al., 2017. Moore, F. C., Baldos, U., Hertel, T. W., and Diaz, D. (2017). New science of climate change impacts on agriculture implies higher social cost of carbon. *Nature Communications*, 8:1601.

Moore et al., 2024. Moore, F. C., Drupp, M. A., Rising, J., Dietz, S., Rudik, I., and Wagner, G. (2024). Synthesis of evidence yields high social cost of carbon due to structural model variation and uncertainties. *Proceedings of the National Academy of Sciences*, 5:e2410733121.

Müller and Watson, 2024. Müller, U. K. and Watson, M. W. (2024). Time varying extremes. *The Review of Economics and Statistics*, pages 1–37.

Nath et al., 2024. Nath, I. B., Ramey, V. A., and Klenow, P. J. (2024). How much will global warming cool global growth? Technical report, National Bureau of Economic Research.

National Association of Insurance Commissioners, 2024. National Association of Insurance Commissioners (2024). Calculation of catastrophe risk charge rcat. Accessed: March 17, 2026.

NOAA, nd. NOAA (n.d.). Severe Weather 101: Flood Types. https://www.nssl.noaa.gov/education/svrwx101/floods/types/. Accessed: 2024-05-22.

NOAA National Centers for Environmental Information, 2026. NOAA National Centers for Environmental Information (2026). U.s. climate regions. https://www.ncei.noaa.gov/access/monitoring/reference-maps/us-climate-regions. Geographical Reference Maps. Accessed: 2026-02-10.

Papke and Wooldridge, 1996. Papke, L. E. and Wooldridge, J. M. (1996). Econometric methods for fractional response variables with an application to 401(k) plan participation rates. *Journal of Applied Econometrics*, 11(6):619–632.

Park et al., 2021. Park, R. J., Behrer, A. P., and Goodman, J. (2021). Learning is inhibited by heat exposure, both internationally and within the united states. *Nature Human Behaviour*, 5:19–27.

Pitman et al., 2022. Pitman, A. J., Fiedler, T., Ranger, N., Jakob, C., Ridder, N., Perkins-Kirkpatrick, S., Wood, N., and Abramowitz, G. (2022). Acute climate risks in the financial system: examining the utility of climate model projections. *Environmental Research: Climate*, 1.

Rennert et al., 2022. Rennert, K., Errickson, F., Prest, B. C., Rennels, L., Newell, R. G., Pizer, W., Kingdon, C., Wingenroth, J., Cooke, R., Parthum, B., Smith, D., Cromar, K., Diaz, D., Moore, F. C., Müller, U. K., Plevin, R. J., Raftery, A. E., Ševčíková, H., Sheets, H., Stock, J. H., Tan, T., Watson, M., Wong, T. E., and Anthoff, D. (2022). Comprehensive evidence implies a higher social cost of co2. *Nature*, 610:687–692.

Rode et al., 2021. Rode, A., Carleton, T., Delgado, M., Greenstone, M., Houser, T., Hsiang, S., Hultgren, A., Jina, A., Kopp, R. E., McCusker, K. E., Nath, I., Rising, J., and Yuan, J. (2021). Estimating a social cost of carbon for global energy consumption. *Nature*, 598:308–314.

Rudik, 2020. Rudik, I. (2020). Optimal climate policy when damages are unknown. *American Economic Journal: Economic Policy*, 12:340–373.

Seneviratne et al., 2021. Seneviratne, S. I., Zhang, X., Adnan, M., Badi, W., Dereczynski, C., Di Luca, A., Ghosh, S., Iskandar, I., Kossin, J., Lewis, S., Otto, F. E. L., Pinto, I., Satoh, M., Vicente-Serrano, S. M., and Wehner, M. (2021). Weather and climate extreme events in a changing climate. In Masson-Delmotte, V., Zhai, P., Pirani, A., Connors, S. L., Péan, C., Berger, S., Caud, N., Chen, Y., Goldfarb, L., Gomis, M. I., Huang, M., Leitzell, K., Lonnoy, E., Matthews, J. B. R., Maycock, T. K., Waterfield, T., Yelekçi, O., Yu, R., and Zhou, B., editors, *Climate Change 2021: The Physical Science Basis. Contribution of Working Group I to the Sixth Assessment Report of the Intergovernmental Panel on Climate Change*, pages 1513–1766. Cambridge University Press, Cambridge, United Kingdom and New York, NY, USA.

Shaw and Stevens, 2025. Shaw, T. A. and Stevens, B. (2025). The other climate crisis. *Nature*, 639:877–887.

Simpson et al., 2024. Simpson, I. R., McKinnon, K. A., Kennedy, D., Lawrence, D. M., Lehner, F., and Seager, R. (2024). Observed humidity trends in dry regions contradict climate models. *Proceedings of the National Academy of Sciences of the United States of America*, 121.

Simpson et al., 2025. Simpson, I. R., Shaw, T. A., Ceppi, P., Clement, A. C., Fischer, E., Grise, K. M., Pendergrass, A. G., Screen, J. A., Wills, R. C. J., Woollings, T., Blackport, R., Kang, J. M., and Po-Chedley, S. (2025). Confronting earth system model trends with observations. *Science Advances*, 11:8035.

Sobel et al., 2023. Sobel, A. H., Lee, C. Y., Bowen, S. G., Camargo, S. J., Cane, M. A., Clement, A., Fosu, B., Hart, M., Reed, K. A., Seager, R., and Tippett, M. K. (2023). Near-term tropical cyclone risk and coupled earth system model biases. *Proceedings of the National Academy of Sciences of the United States of America*, 120.

Swiss Re Institute, 2025. Swiss Re Institute (2025). Growing stronger: How the property & casualty market adapts to a riskier world. sigma report sigma 3/2025, Swiss Re, Zurich, Switzerland.

Trenberth et al., 2003. Trenberth, K. E., Dai, A., Rasmussen, R. M., and Parsons, D. B. (2003). The changing character of precipitation. *Bulletin of the American Meteorological Society*, 84(9):1205–1217.

van den Bremer and van der Ploeg, 2021. van den Bremer, T. S. and van der Ploeg, F. (2021). The risk-adjusted carbon price. *American Economic Review*, 111(9):2782–2810.

Appendix

A Descriptive statistics

Table 2: Descriptive statistics of annual maximum rainfall by city (1970–2024).

City	Mean	SD	Min	Max
Aberdeen	56.30	26.83	19.3	193.5
Abilene	71.87	32.53	34.3	209.8
Akron	58.18	19.81	30.7	122.9
Albany	59.41	20.38	34.0	142.2
Albuquerque	25.21	9.00	12.2	48.8
Amarillo	54.84	22.77	24.1	145.8
Asheville	78.01	22.50	37.6	146.8
Astoria	71.58	21.14	33.3	141.2
Athens	83.78	26.93	42.2	186.4
Atlanta	81.48	27.26	40.1	169.7
Augusta	84.49	25.68	40.9	185.4
Austin	87.83	34.36	37.1	191.8
Bakersfield	21.56	8.03	8.6	58.2
Baltimore	78.08	28.81	43.4	160.0
BatonRouge	122.74	44.70	63.2	285.5
Beckley	54.16	13.98	30.2	91.2
Birmingham	91.96	39.79	47.2	247.7
Bismarck	48.21	22.35	20.3	117.6
Bluefield	54.90	14.52	33.3	91.7
Boise	22.59	7.99	10.9	45.0
Boston	71.46	23.56	37.6	155.2
Buffalo	52.33	20.59	29.0	127.3
Burlington	51.82	13.50	32.3	91.9
CedarRapids	65.92	24.52	32.5	135.9
Charleston	57.45	15.41	27.4	105.4
Charlotte	73.48	27.09	35.6	174.8
Chattanooga	84.79	33.05	48.8	241.0
Cheyenne	37.20	20.36	10.7	153.9

Chicago	71.88	31.51	34.0	174.2
Cincinnati	64.54	16.96	34.3	115.1
CollegeStation	113.20	132.48	24.6	1016.0
ColoradoSprings	48.06	23.79	19.1	114.3
ColumbiaMO	76.90	28.92	0.0	150.9
ColumbiaSC	83.54	26.00	49.8	174.5
ColumbusGA	90.84	28.22	42.2	150.4
ColumbusOH	60.41	14.48	40.4	130.3
CorpusChristi	106.06	45.62	34.8	250.4
DallasFortWorth	78.51	24.20	40.4	148.6
Dayton	57.70	16.94	27.2	96.8
DesMoines	69.68	22.16	39.4	157.0
Detroit	53.90	18.72	32.3	116.1
DodgeCity	59.70	23.65	24.4	120.4
Dubuque	67.44	26.94	31.8	189.7
Duluth	58.30	18.74	28.2	105.2
EauClaire	65.02	24.40	27.7	151.9
Elko	22.64	14.22	10.2	104.9
ElPaso	33.28	12.00	13.7	72.1
Erie	56.11	19.98	27.7	118.4
Eugene	62.14	23.12	31.2	124.2
Eureka	56.51	23.99	25.9	172.5
Evansville	76.71	24.99	36.8	162.6
Fargo	55.82	21.19	11.7	117.9
Flagstaff	47.22	17.14	21.6	99.8
FortMyers	101.85	30.90	55.1	196.9
FortSmith	86.11	26.62	48.5	173.0
FortWayne	58.24	18.63	28.7	111.8
Fresno	31.14	10.36	11.9	60.5
Glasgow	34.42	13.21	12.2	75.2
GlensFalls	59.43	17.12	28.7	93.2
GrandForks	52.94	22.25	21.8	112.8
GrandIsland	60.63	25.89	25.4	165.1
GrandJunction	19.83	6.13	7.6	35.3
GrandRapids	63.41	17.57	34.0	105.4
GreatFalls	33.78	12.51	15.2	72.9
GreenBay	51.35	19.37	24.6	124.5
Harrison	83.05	27.85	46.2	198.9
Helena	24.83	9.02	0.0	49.0
Houston	128.01	65.52	49.3	408.2
Huntington	62.57	14.32	40.6	98.8
Huntsville	90.91	29.38	44.2	230.4

Huron	53.77	19.48	27.7	108.0
Indianapolis	70.04	25.74	40.1	182.9
Jackson	101.72	28.90	54.9	187.5
Jacksonville	105.84	38.57	53.8	198.9
KeyWest	114.50	77.30	39.9	577.9
LaCrosse	64.59	24.89	31.5	142.0
LakeCharles	133.89	60.00	63.0	398.0
Lansing	55.54	18.50	22.9	125.7
Lewiston	21.41	6.75	10.4	45.7
Lexington	76.74	26.02	37.6	141.2
LittleRock	90.95	34.68	48.5	205.7
LosAngeles	54.81	22.86	16.8	141.0
Louisville	77.89	29.15	38.4	183.4
Lynchburg	74.21	25.95	35.6	153.7
Macon	86.91	33.06	42.2	260.4
Madison	64.49	20.34	32.3	114.6
Marquette	54.02	14.30	32.8	109.0
Memphis	90.19	25.19	45.2	149.4
Miami	125.76	65.89	47.0	377.2
Milwaukee	62.38	29.56	26.9	173.0
Minneapolis	63.08	33.27	36.3	232.4
Missoula	23.94	8.63	11.9	51.6
Moline	68.77	23.15	25.4	129.5
Monroe	99.29	41.60	48.0	275.8
Montgomery	92.44	32.84	50.0	207.0
Morgantown	55.54	18.18	28.7	110.0
Muskegon	60.02	20.76	32.0	112.5
Nashville	81.59	28.19	41.4	184.2
NewYork	89.05	34.31	45.0	192.3
NorfolkNE	63.65	22.80	23.6	137.7
NorfolkVA	91.35	40.32	39.9	226.8
NorthPlatte	47.36	14.33	21.8	74.9
Oklahoma	89.30	39.46	32.5	193.5
Omaha	64.56	29.63	28.7	164.1
Pendleton	22.54	7.92	10.9	55.6
Pensacola	141.50	69.22	59.4	395.0
Peoria	61.51	22.22	30.7	131.8
Philadelphia	80.42	33.35	38.9	203.7
Phoenix	29.98	13.88	12.7	83.8
Pittsburgh	55.43	21.20	26.4	151.1
PortlandME	85.55	42.99	38.9	298.2
Pueblo	33.49	13.52	8.1	70.1
Raleigh	82.09	28.31	39.9	163.8

Reno	25.50	11.19	8.6	57.4
Richmond	77.13	31.31	32.8	193.3
RochesterMN	67.18	32.19	25.1	189.7
RochesterNY	51.67	16.75	26.2	88.1
Rockford	70.44	24.99	33.3	144.8
Sacramento	47.23	20.59	15.5	138.2
Saginaw	57.65	25.38	31.5	176.0
SaintCloud	58.53	18.31	27.7	103.6
Salem	47.80	11.66	26.4	78.0
SaltLakeCity	28.36	9.06	12.7	57.7
SanAntonio	97.25	51.69	38.1	286.0
SanDiego	38.55	12.77	18.0	69.3
SaultSteMarie	48.29	22.42	26.9	150.4
Savannah	104.74	42.77	50.0	227.1
Scottsbluff	37.15	13.72	15.0	75.2
Seattle	52.54	18.86	24.1	127.5
Shreveport	98.30	38.63	46.2	265.2
SiouxCity	60.98	21.82	32.3	139.7
SiouxFalls	63.24	24.58	23.1	138.2
SouthBend	65.54	29.90	33.3	195.3
Spokane	23.97	6.57	16.0	55.6
Springfield	71.11	23.60	34.0	142.0
SpringfieldMO	81.49	26.88	42.4	159.3
StLouis	72.31	29.50	37.6	219.5
Tallahassee	115.75	36.48	54.6	207.5
Tampa	98.71	51.52	33.5	290.8
Toledo	54.87	16.47	25.4	86.1
Topeka	71.48	21.00	43.9	142.5
Tucson	35.86	12.51	15.5	75.2
Tulsa	83.75	28.45	43.7	176.5
WashingtonDC	70.34	26.91	31.5	155.2
Waterloo	62.33	20.16	33.5	139.4
Wausau	58.38	17.77	30.7	113.3
WestPalmBeach	124.31	38.70	55.4	223.3
Williamsport	71.90	34.83	29.2	220.0
Wilmington	77.73	31.79	37.6	210.6
Winnemucca	19.63	5.77	8.9	35.1
Worcester	71.60	19.87	38.9	127.0

B Details on Time-Varying Bayesian Model

According to (*Müller and Watson, 2024*), the GEV parameters is are related to the GP parameters (ν, ω, ξ) via $(\mu, \sigma, \xi) = (\omega\frac{n^{\xi}-1}{\xi} + \nu, \omega n^{\xi}, \xi)$. Thus, (μ, σ) may vary in time because the underlying population F has a time varying GP tail, or because the number of observations n is time varying. To isolate these effects, consider the following reparameterization of (μ, σ, ξ) in terms of (ξ, α, s, m): Let $n = n_0\alpha$, where n_0 is of the same order as n, so $\alpha > 0$ captures the sample size relative to the baseline n_0. We have

$$\begin{aligned} \sigma &= (\omega n_0^{\xi})\alpha^{\xi} = s\alpha^{\xi} \\ \mu &= \nu + \omega\frac{(n_0\alpha)^{\xi} - 1}{\xi} = m + s\frac{\alpha^{\xi} - 1}{\xi} \end{aligned} \tag{2}$$

with $s = (\omega n_0^{\xi})$ and $m = \nu + (\omega/\xi)(n_0^{\xi} - 1)$.

The authors model time variation in (μ_t, σ_t) for $t = 1, ..., T$ by independent time variation in (α_t, s_t, m_t) via the mapping (2). Changes in α_t correspond to a time varying number of underlying observations n_t. Time variation in (s_t, m_t), in contrast, corresponds to changes of the GP tail of the underlying population F_t.

The prior on the paths (ξ, α, s, m) is

$$\begin{aligned} &\xi_t = \xi_{min} + (\xi_{max} - \xi_{min})\frac{e^{\bar{\xi}_t}}{1 + e^{\bar{\xi}_t}}, \bar{\xi}_t = \bar{\xi}_0 + \gamma_{\xi}\eta_{\xi,t} \\ &ln(\alpha_t) = ln(\alpha_0) + \gamma_{\alpha}n_{\alpha,t} \\ &ln(s_t) = ln(s_0) + \gamma_s n_{s,t} \\ &m_t = m_0 + \gamma_m n_{m,t} \end{aligned} \tag{3}$$

where the four η_t's are mutually independent random walks with $N(0, 1/T)$ increments and $\eta_0 = 0$, and $\xi_{min} = -0.9$ and $\xi_{max} = 2.1$. For the initial conditions, we choose a $N(0, 1.5^2)$ prior for $\bar{\xi}_0$, which induces a nearly flat prior for $\bar{\xi}_0$ over the $[-0.5, 1.5]$ interval, ln $\alpha_0 = 0$ (a normalization that associates n_0 with the time $t = 0$ value of n), and improper flat priors on ln s_0 and m_0, where these flat priors ensure that Bayesian inference is invariant with respect to location and scale transformations of the data.

The γ parameters govern the degree of time variation in the prior: The difference between the $t = T$ and $t = 0$ value of the (transformed) parameters has standard deviation γ. We use an exponential prior for γ with mean g. In particular, $g_{\alpha} = g_s = 0.5$, so that the mean standard deviation of the change in α and s is 0.5 log points over the sample period. We set $g_{\xi} = 1$; a one unit increase in $\tilde{\xi}$ raises $\xi_0 = 0.5$ to $\xi_T = 0.73$. The parameter m is measured in the same units as the data, and to preserve the invariance, we set $g_m = s_0$.

C Stability test

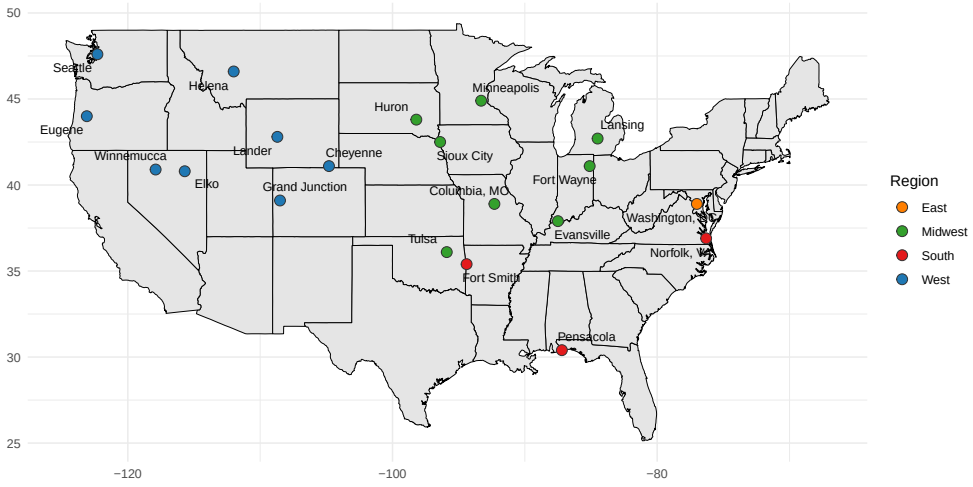


Figure 8: US Cities with Evidence of Max Rainfall Parameter Instability

D Damage Functions

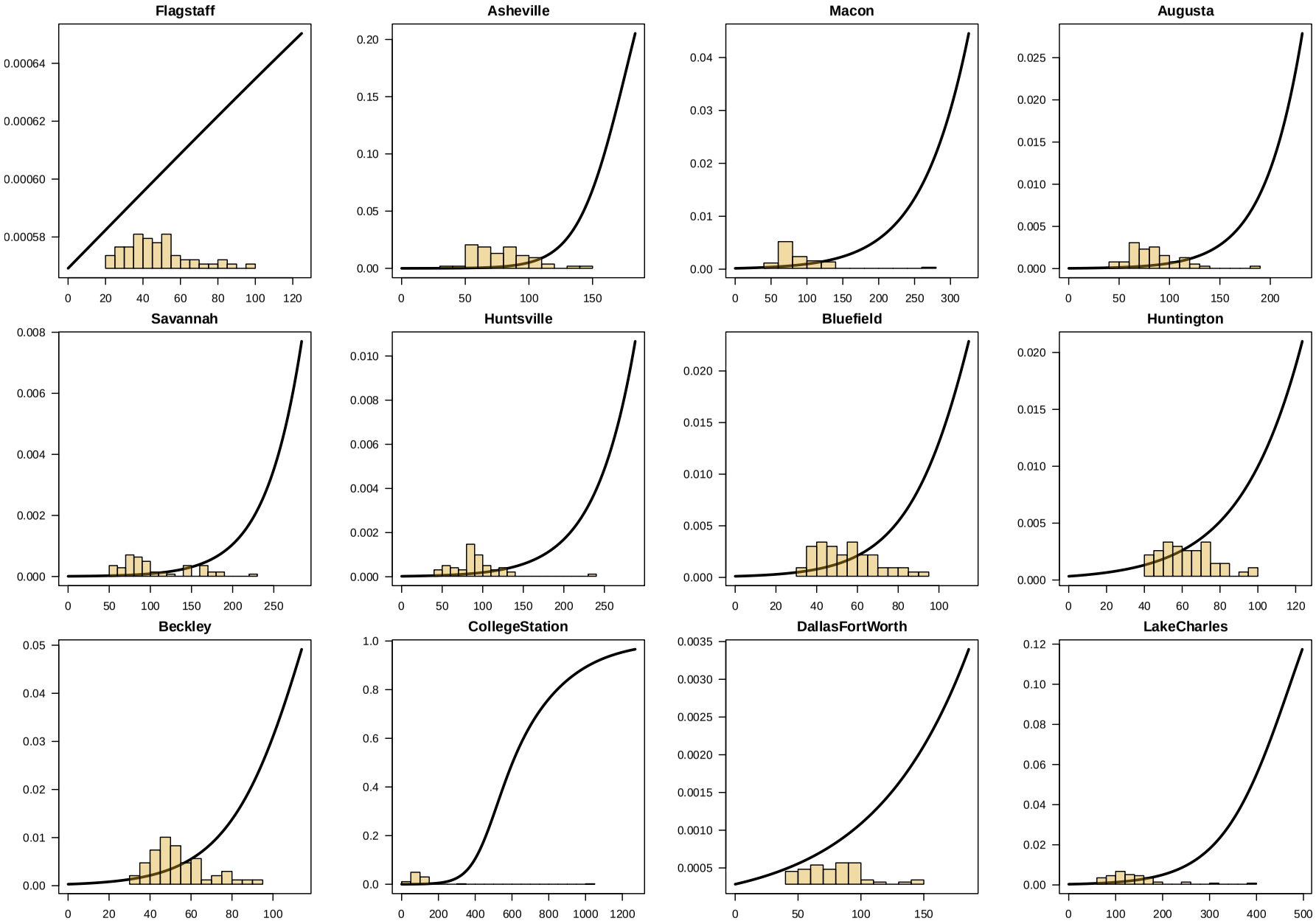


Figure 9: Estimated loss functions for 112 cities retained in the analysis. X axis in all figures is annual maximum daily rainfall (in mm) and y axis is expected loss per policy, as a fraction of building replacement cost.

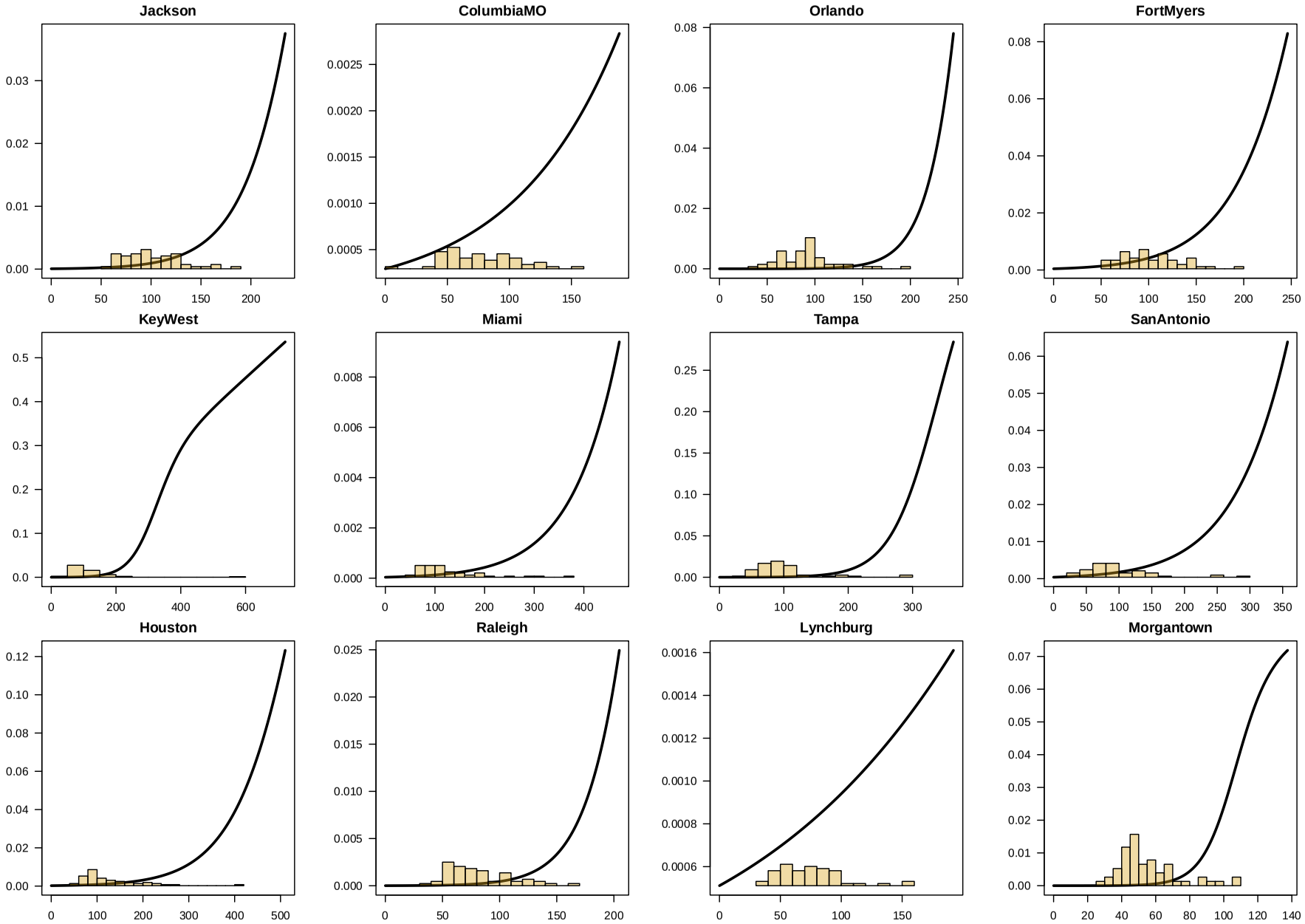


Figure 10: Estimated loss functions for 112 cities retained in the analysis. X axis in all figures is annual maximum daily rainfall (in mm) and y axis is expected loss per policy, as a fraction of building replacement cost.

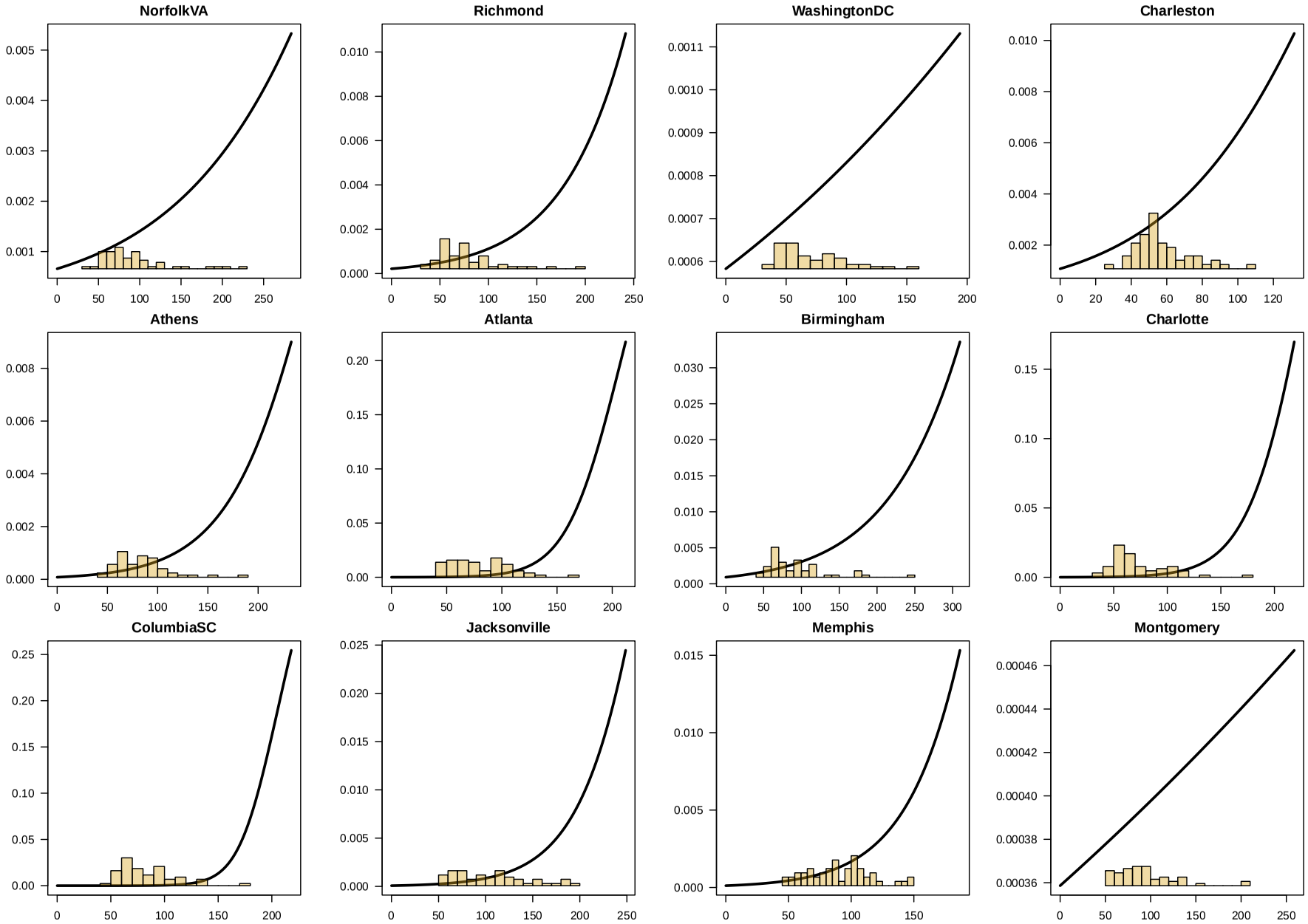


Figure 11: Estimated loss functions for 112 cities retained in the analysis. X axis in all figures is annual maximum daily rainfall (in mm) and y axis is expected loss per policy, as a fraction of building replacement cost.

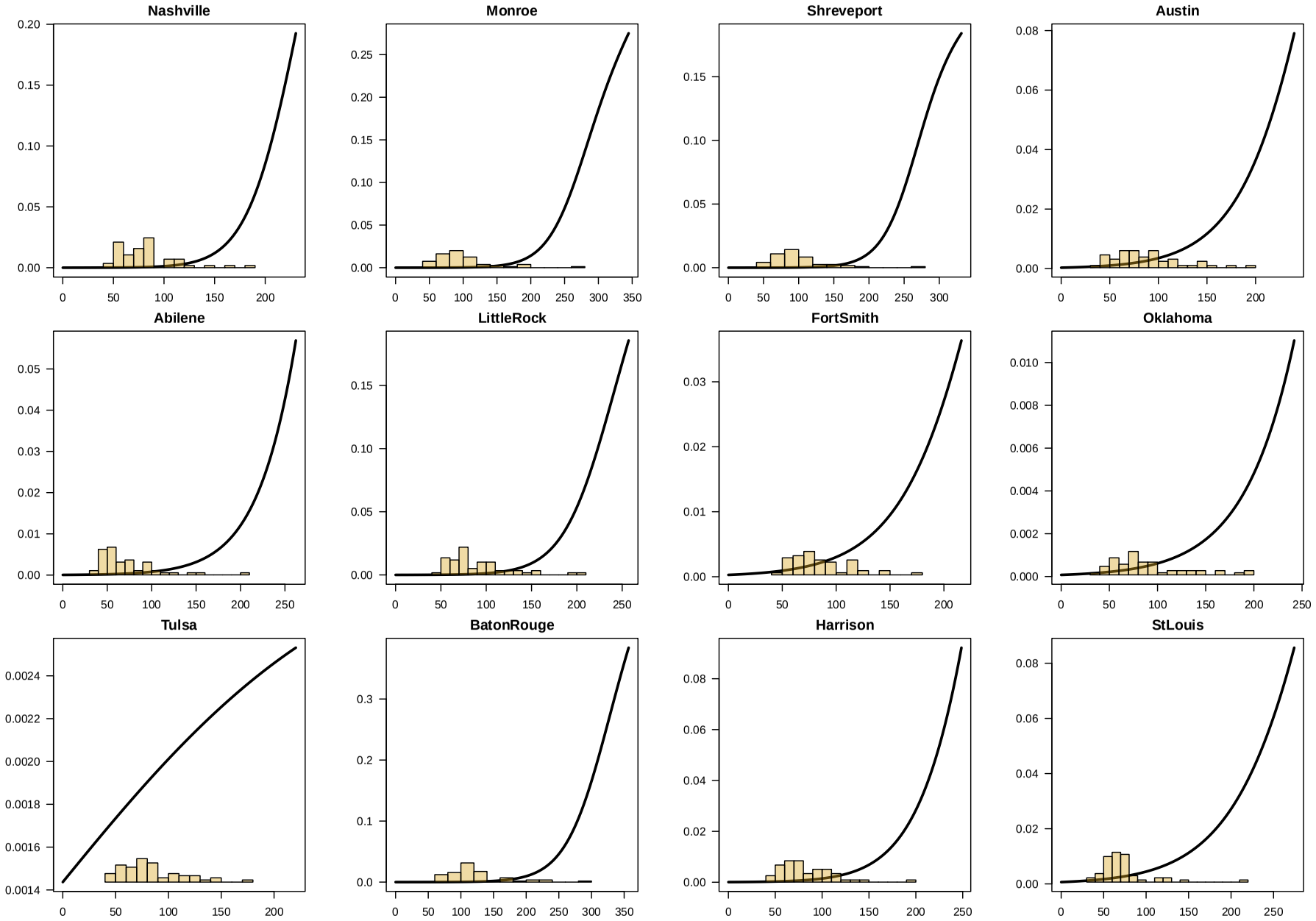


Figure 12: Estimated loss functions for 112 cities retained in the analysis. X axis in all figures is annual maximum daily rainfall (in mm) and y axis is expected loss per policy, as a fraction of building replacement cost.

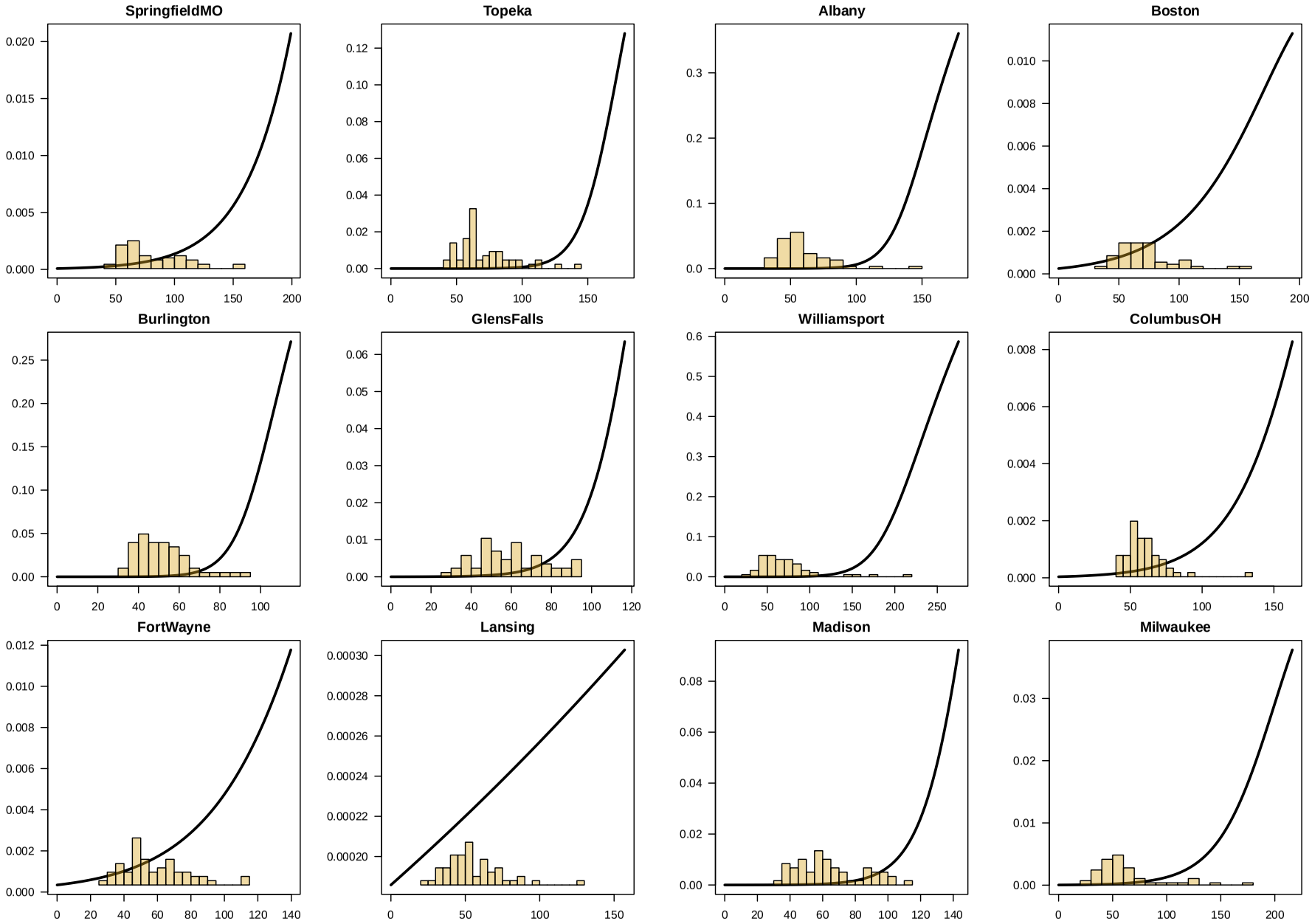


Figure 13: Estimated loss functions for 112 cities retained in the analysis. X axis in all figures is annual maximum daily rainfall (in mm) and y axis is expected loss per policy, as a fraction of building replacement cost.

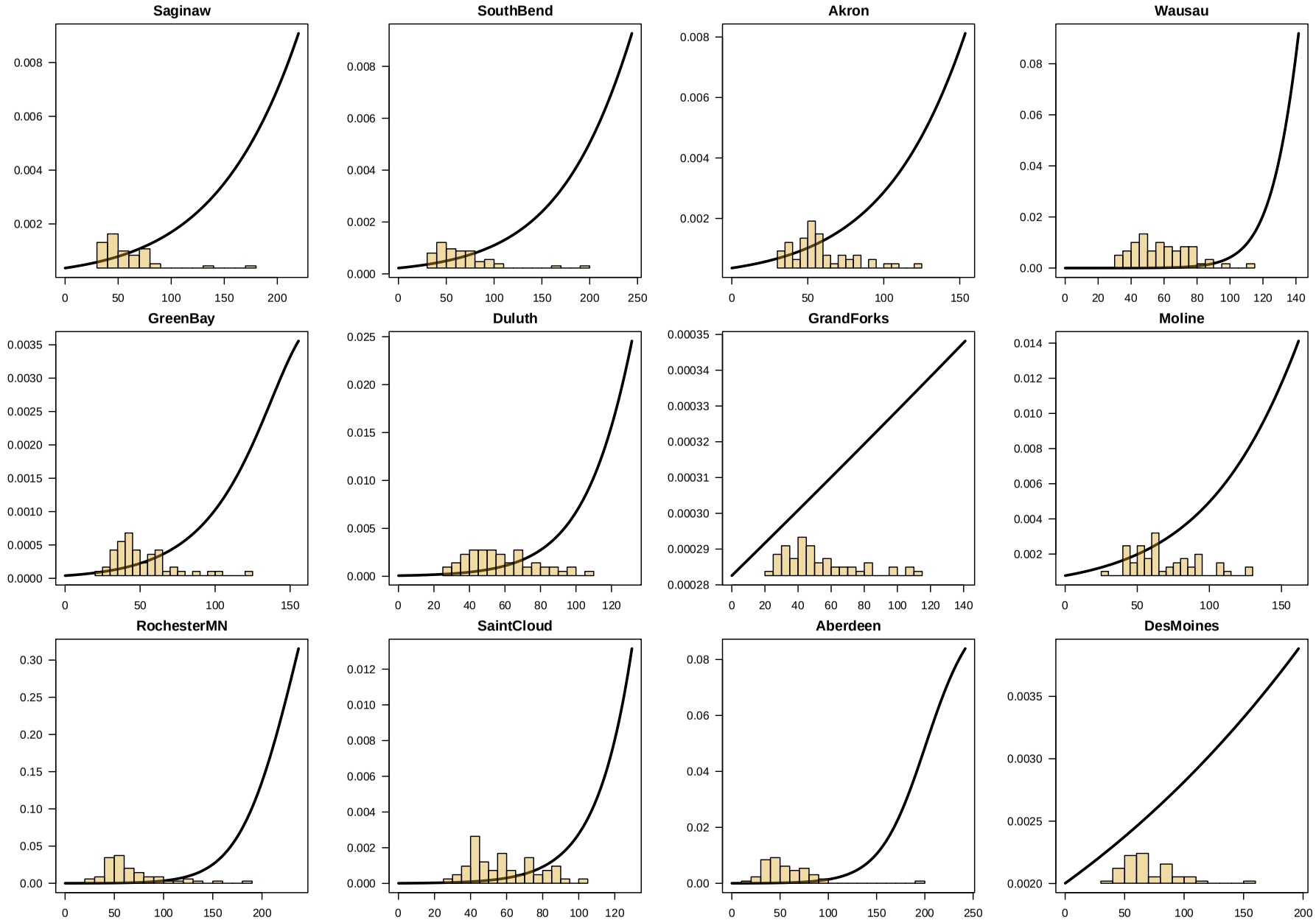


Figure 14: Estimated loss functions for 112 cities retained in the analysis. X axis in all figures is annual maximum daily rainfall (in mm) and y axis is expected loss per policy, as a fraction of building replacement cost.

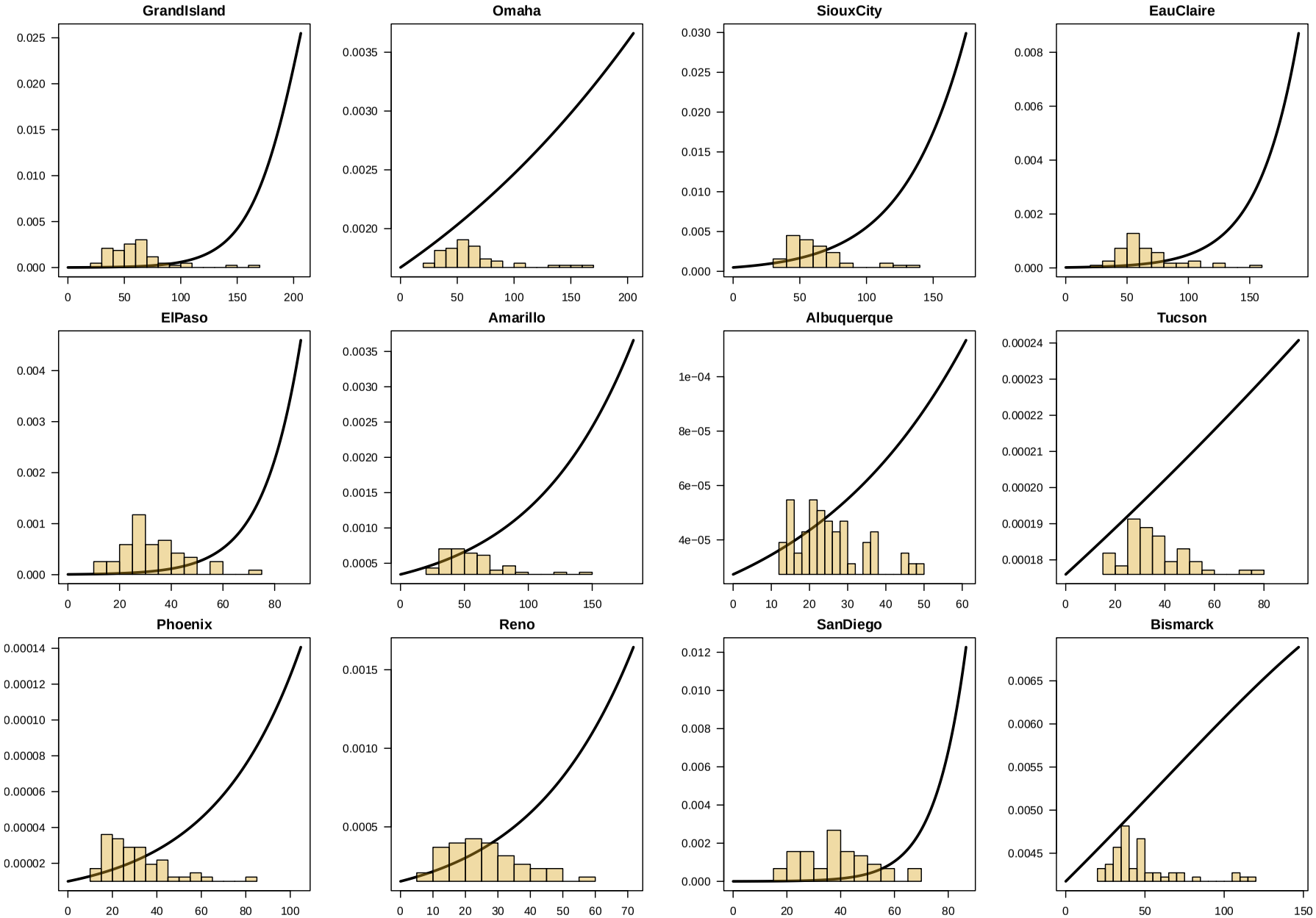


Figure 15: Estimated loss functions for 112 cities retained in the analysis. X axis in all figures is annual maximum daily rainfall (in mm) and y axis is expected loss per policy, as a fraction of building replacement cost.

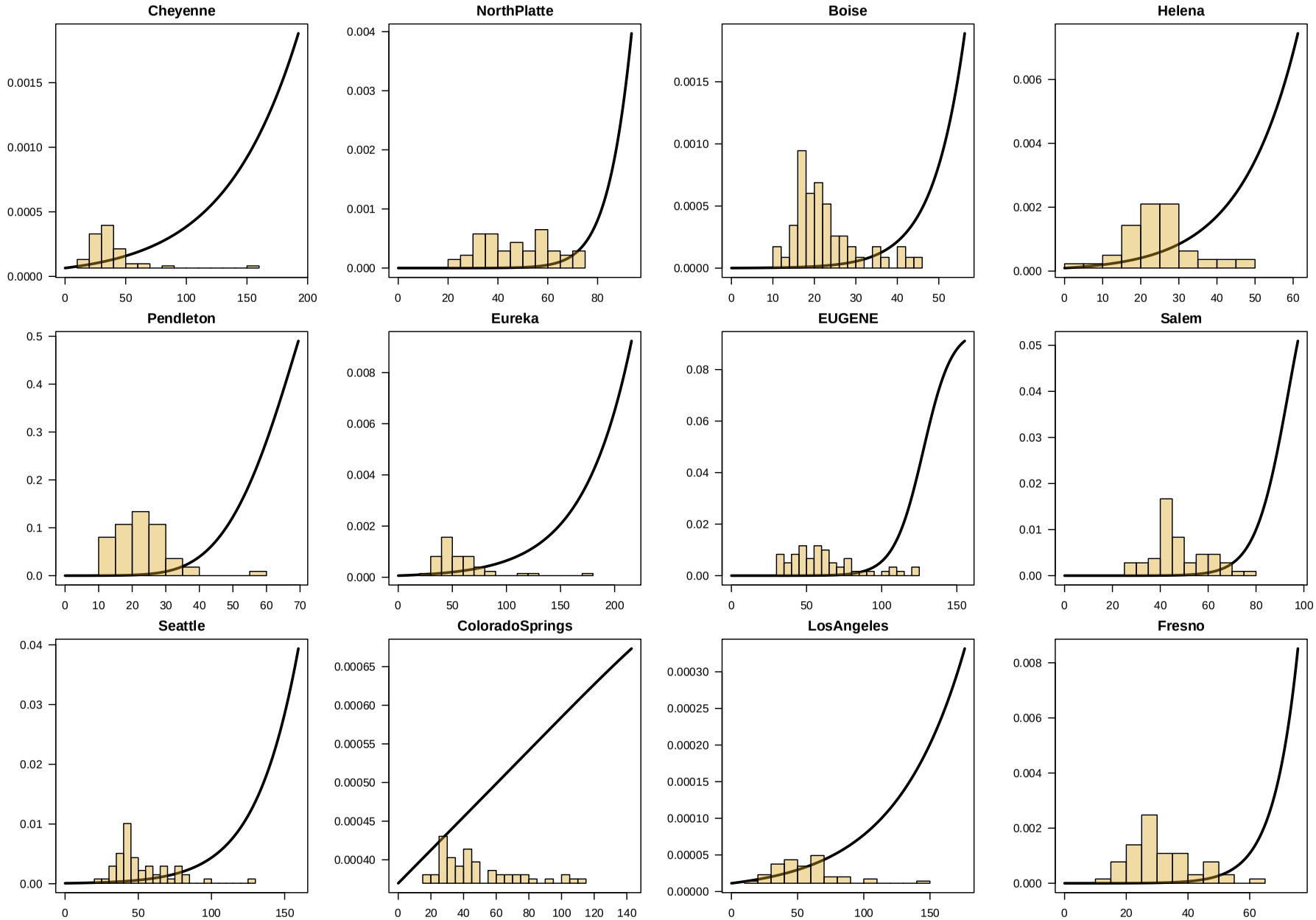


Figure 16: Estimated loss functions for 112 cities retained in the analysis. X axis in all figures is annual maximum daily rainfall (in mm) and y axis is expected loss per policy, as a fraction of building replacement cost.

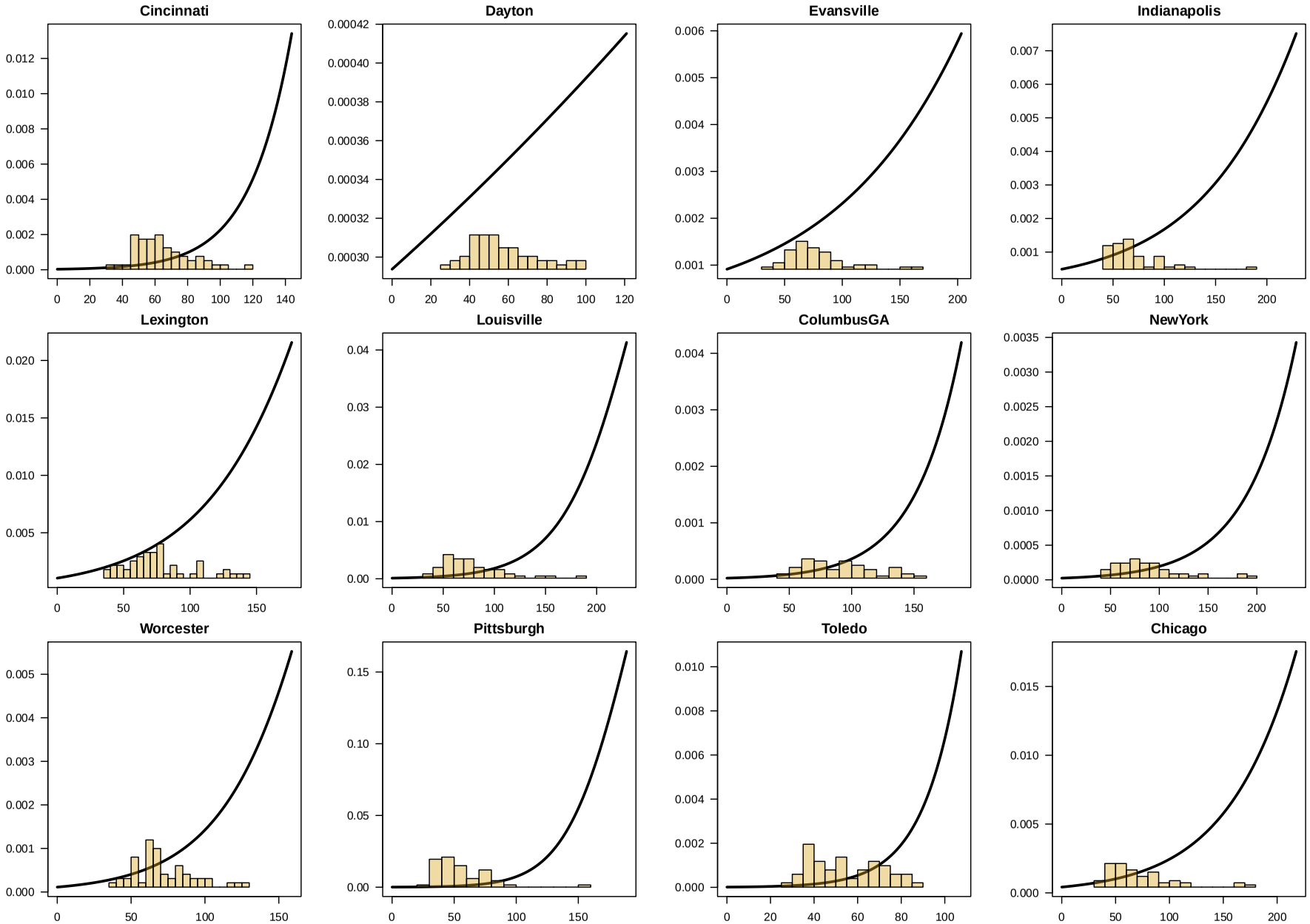


Figure 17: Estimated loss functions for 112 cities retained in the analysis. X axis in all figures is annual maximum daily rainfall (in mm) and y axis is expected loss per policy, as a fraction of building replacement cost.

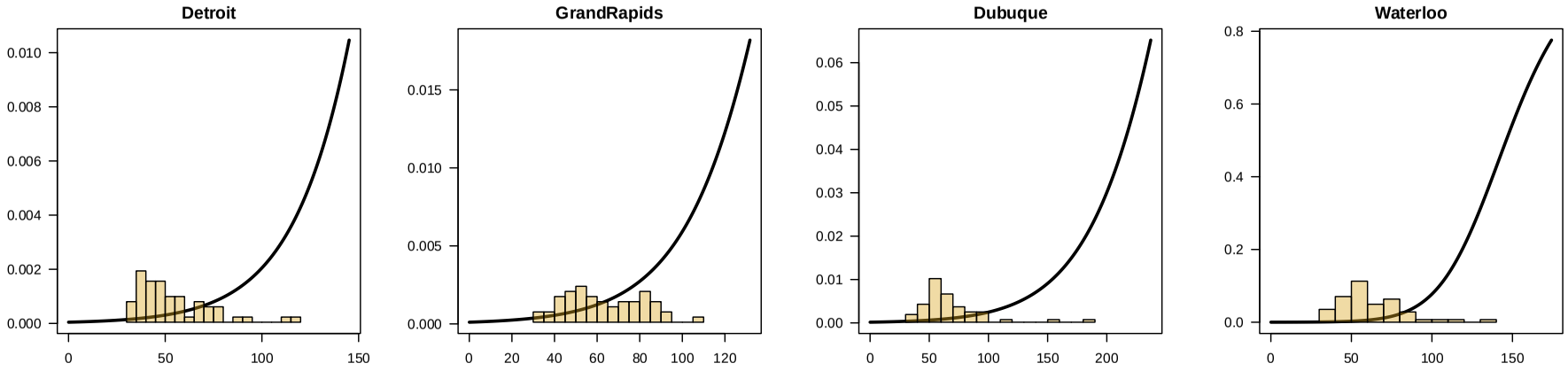


Figure 18: Estimated loss functions for 112 cities retained in the analysis. X axis in all figures is annual maximum daily rainfall (in mm) and y axis is expected loss per policy, as a fraction of building replacement cost.

E Extreme Rainfall Correlations Among Cities

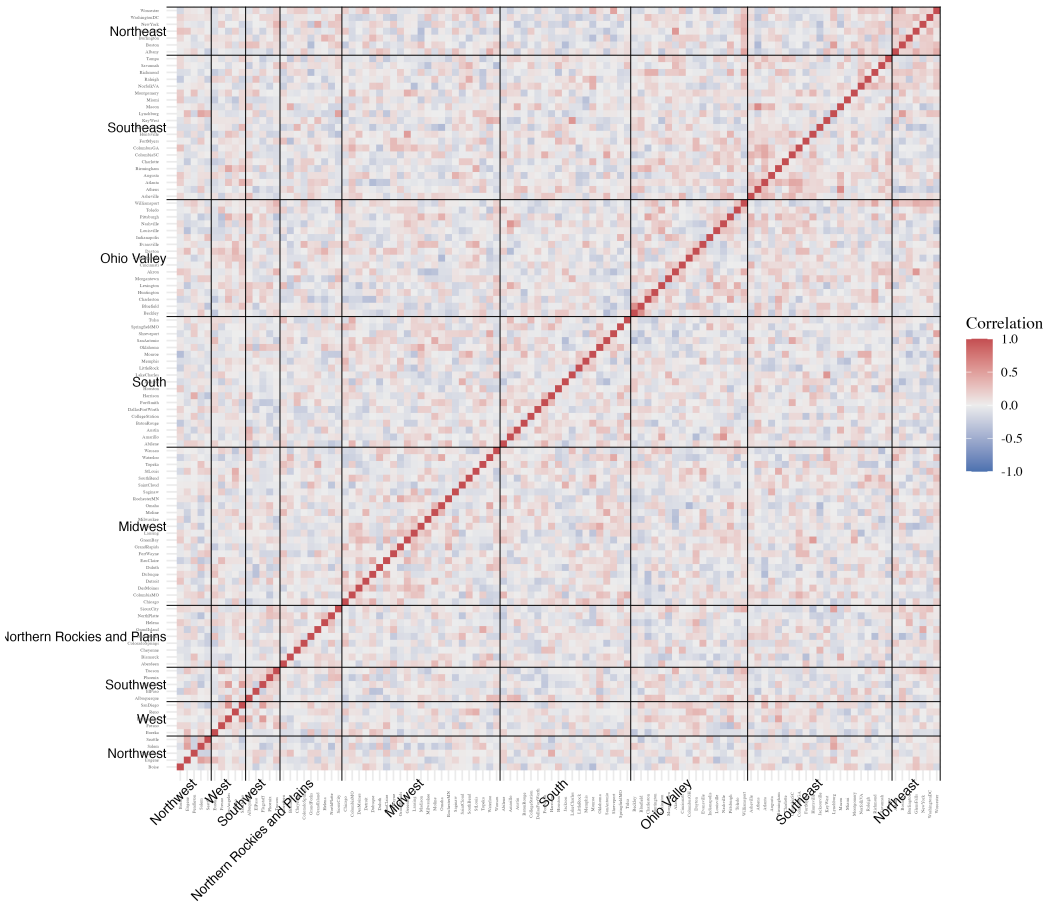


Figure 19: **Regional Patterns of Correlated Rainfall Extremes in the United States.** Correlations are calculated on annual rainfall isolated using a Hodrick-Prescott (HP) filter with a smoothing parameter of $\lambda = 100$. This procedure removes long-term climate trends to ensure that spatial dependencies reflect synchronized meteorological shocks rather than a common drift in the distribution mean.